APPLICATIONS OF PLASMA DENSITY MEASUREMENTS TO SPACECRAFT RADIO TRACKING

by

Thomas Marshall Eubanks

B.S., Massachusetts Institute of Technology (1977)

SUBMITTED IN PARTIAL FULFILLMENT
OF THE REQUIREMENTS OF THE
DEGREE OF
MASTER OF SCIENCE

at the

MASSACHUSETTS INSTITUTE OF TECHNOLOGY

June 1980

Signature of Author _____
Department of Earth and Planetary Sciences
May 26, 1980

Certified by _____ / _____
Irwin I. Shapiro
Thesis Supervisor

Accepted by _____
Chairman, Departmental Graduate Committee

APPLICATIONS OF PLASMA DENSITY MEASUREMENTS TO SPACECRAFT RADIO TRACKING

by

Thomas Marshall Eubanks

Submitted to the Department of Earth and Planetary Sciences on May 26, 1980 in partial fulfillment of the requirements for the degree of Master of Science.

ABSTRACT

S-band plasma delays are estimated as part of a test of the general relativistic time delay effect conducted during the Viking Mission to Mars. The processing of radio tracking data taken with the Viking Orbiters and Landers is discussed. The statistical properties of Viking Orbiter dual-frequency delay and Doppler measurements are described. It was concluded that the plasma delay can be adequately modeled as a random walk. The implications of this model on estimation of Viking Lander plasma delays are discussed. The results of use of the random walk model for Viking lander plasma delay correction are compared with the results from other plasma models, and it is concluded that this model is sufficient for estimation of Viking Lander plasma delays.

Thesis Supervisor: Dr. Irwin I. Shapiro

Title: Professor of Physics and Geophysics

TABLE OF CONTENTS

Chapter I

Introduction

In the past twenty years, advances in many fields have made possible an enormous increase in the accuracy of measurements of positions and velocities of objects in the inner solar system. An important factor in this progress has been the placement of probes throughout the solar system during the program of interplanetary exploration initiated by the United States in the early 1960's.

Radio tracking using spacecraft transponders makes possible accurate measurements of delays and Doppler shifts of signals propagating between a ground station and the spacecraft. With probes in interplanetary space, the solar system can be used as a vast laboratory for gravity research, including research on general relativity and the dynamical properties of the planets. The solar system, not being under the control of the experimenter, is poorly designed for such experiments. One major complication to the interpretation of present day radio tracking data is the effect of the interplanetary medium on propagating radio waves. The estimation of the total plasma delay for delay observations from one spacecraft given downlink only measurements of the plasma delay from another spacecraft is the major experimental problem addressed in this thesis. This work was done in connection with a test of general relativity conducted during the Viking mission to Mars (reference 1).

At present, the solar system is used for the most definitive tests of general relativity. As was first shown by I. I. Shapiro in 1964 (reference 21), the mass of the sun causes an increase in the radio propagation delay over that expected from Euclidean geometry. The maximum excess relativistic delay occurs at superior conjunction, when the sun moves directly between the earth and Mars and the raypath passes close to the sun. For Viking, the delay at that time is about 250 microseconds (μsec) while the corresponding total round trip delay is about 2500 seconds. Unfortunately, the plasma effect is also at a maximum at superior conjunction, with the greatest measured plasma delay being on the order of 100 μsec at a radio wavelength of 12 cm. Accurate estimates of the plasma delay are thus vital to the general relativity experiment.

The Viking spacecraft and ground equipment make it possible, under good conditions, to measure the Earth-Mars round trip radio propagation time with an uncertainty of about 10 nanoseconds (nsec) and the carrier frequency Doppler shift with an uncertainty of on the order of 1 mHz. The propagation medium makes it impossible to infer the vacuum range and line-of-sight velocity to that accuracy, and currently constitutes the largest source of error in the interpretation of interplanetary radio tracking data.

The propagation effects from the medium between the Earth and Mars are dominated, at radio frequencies, by the

contribution from the interplanetary plasma in the solar corona. The other major parts of the propagation medium are the terrestrial atmosphere and ionosphere. The dual-frequency data includes a contribution from the ionosphere but not from the non-dispersive contribution from the Earth's neutral atmosphere.

The solar plasma is a highly dispersive medium. The excess plasma delay or Doppler shift is proportional to the inverse square of the carrier frequency, and to the local plasma density. The solar wind is very complex, with density fluctuations at times of the order of the mean. It is impossible to adequately estimate the solar plasma delays purely from a time averaged density model, as is done with the terrestrial atmosphere propagation delays. To model the solar wind from first principles would probably be more difficult than modeling the weather on Earth. It is thus necessary to consider statistical models of the plasma delay and delay rate, similar in spirit to the models discussed in references 13 and 14.

This thesis is concerned with Viking Orbiter and Lander radio tracking data taken between July 20, 1976 and September 3, 1977. Viking Lander (VL) 1 and Viking Orbiter (VO) 1 were launched as a single spacecraft on 20 August 1975 and were inserted into Martian orbit on 19 June 1976. VL2 and VO2 were launched together on 9 September 1975 and were inserted into Martian orbit on 7 August 1976. VL1 landed on the

surface of Mars on 20 July followed by VL2 on 3 September 1976. As of January 1980, VO2 is inactive and VL2 is incapable of communicating directly with Earth and is unable to take part in these radio tracking experiments.

The Landers are equipped for interplanetary radio tracking at S-band (12 cm) only. The Orbiters have, in addition, a coherent dual-frequency downlink, at S-band and X-band (2.3 cm). Differenced dual-frequency (S-band minus X-band or SX) measurements can provide estimates of the time delay and Doppler shift contributions from the interplanetary plasma.

On November 25, 1976 and again on January 21, 1979, the earth and Mars (together with the Viking spacecraft) passed through superior conjunction. The plasma and relativistic effects are at a maximum near superior conjunction, while the signal-to-noise ratio is lowest there (due to plasma attenuation and solar radio interference). Despite this, it was possible to track the Viking spacecraft to within 2 or 3 days before and after superior conjunction.

The SpaceCraft (S/C) numbers are used as an alternate designation for the Viking spacecraft:

VL1 = S/C 26

VO1 = S/C 27

VL2 = S/C 29

VO2 = S/C 30

The Orbiters are subject to unmodeled accelerations such as gas leaks from the attitude control system, which compli

cate the interpretation of Orbiter range and Doppler data. The Orbiter SX data are not affected by the motion of the Orbiter, since the range or Doppler shift to the spacecraft cancels out in the differencing. The Landers, which cannot make dual-frequency measurements, are fixed on the surface of Mars, which is nearly free from stochastic accelerations. It is thus necessary to estimate plasma corrections for the Lander delay measurements for both the uplink and downlink from Orbiter downlink dual-frequency measurements.

Chapter II will discuss the basic observables, the differenced observables that can be constructed from them, and how the measurements are made. Chapter III discusses the computer processing required before the dual-frequency Orbiter data can be used to obtain plasma delays. Chapter IV gives the results of a statistical study of the plasma data, and Chapter V describes the application of these results to Lander range measurements.

Chapter II

The Observables

A. Introduction

Radio tracking of interplanetary spacecraft provides two observables, the round trip propagation (group) delay and the Doppler shift of the carrier frequency. The group delay and Doppler shift are a function of the group and phase velocities, respectively, in the propagation medium along the signal path. In a tenuous plasma, such as the solar corona, the phase and group velocities are displaced by opposite and nearly equal amounts from c, the velocity of light. The phase velocity is greater than the group velocity, which is the velocity of energy and information transfer in the medium (reference 6).

In a tenuous plasma, the group and phase velocities can be approximated by

$$v_{phase} = c\left(1 + \frac{aN_e}{2f^2}\right) \qquad (2.1a)$$

and

$$v_{group} = c\left(1 - \frac{aN_e}{2f^2}\right) \qquad (2.1b)$$

where c is the velocity of light in a vacuum, f is the carrier frequency (Hz), a is a constant equal to $8.1 \cdot 10^7$, and N_e is the electron density in electrons cm^{-3}.

On Earth, the solar corona would be considered a very good vacuum, but the coronal plasma can contribute up to 100 μsec to the total S-band range delay near superior conjunction. The coronal plasma density is notoriously hard to model and shows fluctuations exceeding the mean in some cases. This difficulty is especially severe for the Viking relativity experiment, which is most sensitive to delay range measurements taken near superior conjunction. The Viking Orbiters have the ability to retransmit a received S-band ranging code coherently at both S-band and X-band. Dual-frequency measurements of the group delay and Doppler shift using the Viking Orbiters are used to estimate Viking Lander plasma delays, and improve estimates of the true range to the Landers.

In this chapter I will first discuss the nature of the observables, both the delay and Doppler shift and the differenced dual-frequency observables, including the connection between the observables and the propagation medium. In the second part of this chapter, I will discuss the techniques and equipment used to make observations with the Orbiters and the Landers. The next chapter concerns the computer processing required to handle the mass of dual-frequency data available from the Viking experiment.

B. The Propagation of Electromagnetic Waves in a Plasma

In a vacuum, there is only one velocity of propagation of an electromagnetic signal, c. In a neutral medium, such

as the Earth's atmosphere, the velocity of propagation is somewhat less than c. In a tenuous plasma, there are (at least) two velocities of propagation, the group and the phase velocity. The group velocity is the velocity of propagation of wave packets or of modulation of the carrier; the group delay is the round-trip propagation time. The phase velocity is the velocity of propagation of wave crests. Since each wave crest is indistinguishable (the phase can only be measured modulo 2π), the total phase delay cannot be measured, only the change in the phase delay over a measurement interval. The concepts of group and phase velocities and the expressions derived for them are approximations, which become less valid as the plasma density or external magnetic field strength increases. In Section B.2 I will show that these approximations are precise enough for the Viking radio propagation experiments. (Section 1 is adapted from references 6 and 7.)

1. The Definition of the Group and Phase Velocity

Assume that at time to wave packet can be described by $\underline{u}(\underline{x},t_o)$ which has Fourier transform of

$$\underline{A}(k) = \frac{1}{\sqrt{2\pi}}\int_{-\infty}^{\infty} \underline{u}(\underline{x},t_o)e^{-i\underline{k}\cdot\underline{x}}d^3\underline{x} \qquad (2.2)$$

Here $\underline{k}$ is the wave vector, in units of cm^{-1}, k is the magnitude of $\underline{k}$, and the wavelength, λ, is $2\pi/k$. The general solution to the Helmholtz wave equation for a traveling wave is

$$\underline{u}(\underline{x},t) = \frac{1}{\sqrt{2\pi}}\int_{-\infty}^{\infty} \underline{A}(\underline{k}) e^{i\underline{k}\cdot\underline{x} - itw(k)} d^3\underline{k} \qquad (2.3)$$

where w is the angular frequency associated with the wavenumber k. In a vacuum, w is equal to ck, but, in general, w is a function of k. The phase velocity is defined as

$$v_{phase} = \frac{w(k)}{k} \qquad (2.4)$$

In a tenuous plasma, $v_{phase} > c$ and, in a neutral medium, $v_{phase} < c$. Although the phase velocity can be greater than c, information is propagated at the group velocity, which is less than c, and the postulates of special relativity are not violated.

If the wavenumber distribution $\underline{A}(\underline{k})$ of some signal is compact and centered about some value $\underline{k}_0$, then $w(\underline{k})$ can be expressed as a Taylor series expansion in k:

$$w(\underline{k}) = w(\underline{k}_0) + \left.\frac{dw}{d\underline{k}}\right|_{k_0} (\underline{k} - \underline{k}_0) + \text{higher order terms} \qquad (2.5)$$

Ignoring the higher order terms, the integral in Equation 2.3 can be performed to give

$$\underline{u}(\underline{x},t) \approx e^{it(\underline{k}\left.\frac{dw}{d\underline{k}}\right|_{\underline{k}_0} - w(\underline{k}_0))} \underline{u}(\underline{x} - \left.\frac{dw}{d\underline{k}}\right|_{\underline{k}_0} t, t_o) \qquad (2.6)$$

A comparison with the original signal $u(x,t_o)$ shows that, to within a phase factor, the wave packet travels undisturbed at the group velocity, which is thus defined to be

$$v_{group} \equiv \left.\frac{dw}{d\underline{k}}\right|_{\underline{k}_0} \tag{2.7}$$

If the higher order terms in the expansion of w(k) are important, then the wave packet will change shape as it travels and the group velocity may lose much of its meaning.

2. Group and Phase Velocity in the Coronal Plasma

The solar corona consists largely of ionized hydrogen, with about 4% ionized helium by weight and essentially no neutral component. This plasma is so tenuous (about 10 electrons cm^{-3} at 1 A.U.) that interactions between particles in the gas can be ignored, and it can be treated as a sea of free particles. Although the solar wind has temperatures on the order of 10^{6}°K, it is not a relativistic medium, since thermal velocities are on the order of only 4000 km sec^{-1} for electrons at that temperature. Thus classical electrodynamics can be used to treat radio propagation in the solar corona. The following discussion is adapted from reference 7, page 210 and following.

Let $\underline{r}$ describe the position of a particle, p, in a coordinate system centered upon the instantaneous equilibrium position of p. Under the influence of a propagating radio wave, the equation of motion of p is

$$m\frac{d^2\underline{r}}{dt^2} - \frac{e}{c}\underline{B} \times \frac{d\underline{r}}{dt} \simeq -e\underline{E} \qquad (2.8)$$

where m and e are the particle's mass and charge, respectively, $\underline{B}$ is the external magnetic field parallel to the direction of propagation (assumed to be a constant), and $\underline{E}$ is the transverse electric field of the propagating wave. (Notice that we are ignoring the transverse magnetic field of the radio wave, as well as particle interactions.)

Equation 2.8 can be solved to yield

$$\underline{r} = e\left(\frac{1}{mw(w \pm w_b)}\right)\underline{E} \qquad (2.9)$$

where $w_b = e|\underline{B}|/(mc)$ is the frequency of precession of the particle in the external magnetic field, called the cyclotron frequency. The displacement of all charged particles in the plasma gives rise to a net dipole moment and thus to a macroscopic dielectric constant of

$$\xi = 1 - \frac{w_p^2}{w(w \pm w_b)} \qquad (2.10)$$

where

$$w_p = \left(\frac{4\pi ne^2}{m}\right) 1/2$$
$$= 5.64 \cdot 10^4 \sqrt{n} \text{ radians sec}^{-1} \text{ (for electrons)} \qquad (2.11)$$

is called the plasma frequency, and n is the particle number density (particles cm^{-3}). (The ± in Equation 2.10 and 2.11 refers to the two senses of circular polarization.)

The relation between w, ξ, and the wavenumber k is

$$w = \frac{kc}{\sqrt{\xi}} \tag{2.12}$$

Using the definitions given in Equation 2.4 and 2.7 and expanding in a power series in w_p and wb, we get

$$v_{phase} = \frac{w}{k} \simeq c\left(1 + 1/2\frac{w_p^2}{w^2}\left(1 \pm \frac{w_b}{w} + \frac{w_b^2}{w^2} \pm \ldots\right) + 1/4\frac{w_p^4}{w^4} + \ldots\right) \tag{2.13a}$$

$$v_{group} \simeq c\left(1 - 1/2\frac{w_p^2}{w^2}\left(1 \pm 2\frac{w_b}{w} + 3\frac{w_b^2}{w^2} \pm \ldots\right) - 1/8\frac{w_p^4}{w^4} + \ldots\right) \tag{2.13b}$$

and

$$T \equiv \frac{d^2w}{dk^2} \simeq +\left(\frac{w^3}{cw_p^2}\right)^{-1} \tag{2.13c}$$

The first order terms in w_b correspond to Faraday rotation. T is the next term in the expansion of w(k), and is a measure of the distortion in a propagating wave packet. I will show that the second-order term in w_p dominates, and that T, the distortion term, is negligible.

Clearly the higher order terms will be more important as the plasma density increases. At S-band, w is $2\pi \cdot 2.3 \cdot 10^9$ radians sec^{-1} and Δk is equal to $4 \cdot 10^{-4}$ radians cm^{-1}. At 5 solar radii ($R_\odot$), which is as deep as the Viking data probes the solar wind, the average plasma density is 10^5 electrons/cm^3 and the average magnetic field is about 1 Gauss. Under these conditions, $w_p = 2 \cdot 10^7$ radians sec^{-1} and $w_b = 2 \cdot 10^7$ radians sec^{-1}. Thus, considering the electrons only,

$$\frac{w_p^2}{w^2} = 1.5 \cdot 10^{-6} \qquad (2.14a)$$

$$\frac{w_b}{w} = 1.2 \cdot 10^{-3} \qquad (2.14b)$$

and

$$T\Delta k = 10^{-9} << v_{group} \simeq c \qquad (2.14c)$$

Only the first term in w_p need be retained.

To first order, therefore, the group and phase velocity differ by equal but opposite amounts from c. Note that the group velocity, the velocity of information transport in a tenuous plasma, is less than c, as expected. For the rest of this thesis, we will assume that the group and phase velocity in the solar wind are given to sufficient accuracy by Equation 2.1a and Equation 2.1b.

In this part of this chapter, we have used CGS units. From now on we will use natural units in which c = 1. If $f = w/2\pi$ is the radio carrier frequency, then

$$v_{phase} = 1 + 4.03038 \cdot 10^7 \frac{n_e}{f^2} \qquad (2.15a)$$

and

$$v_{group} = 1 - 4.03038 \cdot 10^7 \frac{n_e}{f^2} \qquad (2.15b)$$

with n_e in electrons cm^{-3}.

C. Group Delays and Doppler Shifts Caused by the Solar Wind

If R is the true range delay, the measured delay, τ, will be

$$\tau_m = \int_0^R \frac{ds}{v_{group}} \simeq \int_0^R ds\left(1 + \frac{w_p^2}{2w^2}\right) \qquad (2.16)$$

Let

$$P = \frac{(e_p^2)}{2m_p\pi}\int_0^R n_e ds = 0.03038 \quad 10^7 \int_0^R n_e ds \qquad (2.17)$$

P is proportional to the integrated columnar content (the $\int_0^R n_e ds$) thus

$$\tau_m \simeq R + P/f^2 \qquad (2.18)$$

R is independent of f, and therefore P can be estimated if τ_m is measured for two different frequencies.

The derivation of the Doppler phase delay proceeds in much the same fashion as that of the group delay. The total phase delay cannot be measured, only the relative delay from the start of the observation session or pass. Since it is not possible to continuously monitor the phase delay from the start of the mission, the total phase delay is unknown. If τ_p is the phase delay at the ground station, then the Doppler shift measured, D_m, is

$$D_m = \frac{d\tau}{dt}P = \left(\frac{dR}{dt} - \frac{1}{w^2}\frac{dP}{dt}\right) \qquad (2.19)$$

From dual-frequency Doppler measurements, dP/dt can be inferred. It is possible in theory to use SX range measurements to find the initial value for P, and to use the more

accurate Doppler measurements to estimate the change in P. This process is called Range Integrated Doppler (or RID) and provides the most accurate estimates of P. Unfortunately, the cycle slip problem, which is discussed in Chapter III. D, has prevented use of the Doppler measurements, and the potential accuracy of RID measurements has yet to be achieved.

1. The Thin Screen Model of the Solar Plasma

The Viking Orbiters can be used to measure the plasma delay over the downlink only. The measured range must be corrected for plasma delays for both the uplink and the downlink, and thus the uplink plasma delay must be calculated from downlink plasma delay measurements. The static (or $P_{up} = P_{down}$) model assumes that the uplink plasma delay, P_{up}, is the same as the (measured) downlink delay, P_{down}. In order to find a better approximation to P_{up}, it is necessary to consider some model of the solar corona and of the measurement.

Experimental studies (reference 20) using both ground-based and in situ spacecraft measurements show that the long term average coronal electron number density can be modeled by

$$n_e(r) = \frac{1.55\ 10^8}{r^6} + \frac{3.0\ 10^6}{r^{2.4}} \text{ electrons cm}^{-3} \qquad (2.20)$$

where r is in solar radii. If we use Equation 2.21 as a model of the local plasma density, it is clear that the major contribution to the integrated plasma density will come from

near the thin-screen point, the point on the raypath closest to the sun. Figure 1 shows the observation geometry. The vacuum delay is

$$R_i = R_{up} + R_{down} = (A_i + B_i) + (C_i + D_i) \qquad (2.21)$$

P_1 and P_2 are called the thin-screen points. P_2' is the thin-screen point for the downlink matched to the ith uplink. Each thin-screen point has a location in time as well as in space, and the ith thin-screen time is the time at which the signal passes through P_i. P_1 and P_2' are matched in time, and the spatial separation between thin-screen points is ignored. The thin-screen model assigns all of P_{up} to P_1 and P_{down} to P_2 and ignores contributions from other parts of the raypath. This model is most realistic near superior conjunction, when the raypath nearly grazes the limb of the sun. Far from superior conjunction, the thin-screen model is irrelevant since at such times the plasma delay and delay rate are small and changing slowly.

In our implementation of the thin-screen model, we assume that P_1 is coincident with P_2', which amounts to ignoring the distance between P_1 and P_2' and any asymmetry in the plasma contributions away from the thin-screen point (which would contribute at different times to P_{up} and P_{down}). R_i is an estimate of the delay at time t_i. Near superior conjunction, we can use R_i to approximate the thin-screen

delay Δt_{ts}. If R_e ($\simeq$ 1 A.U.) is the distance between the Earth and the sun at t_i and R_m ($\simeq$ 1.5 A.U.) is the Mars-Sun distance at t_i, then

$$C_i \simeq \frac{1}{2R_i}(R_i^2 + R_m^2 - R_e^2) \qquad (2.22)$$

Assume that $C_i = B_i$; if Δt_{ts} is the thin-screen delay then

$$\Delta t_{ts} = t - t_{ts} = C_i + B_i \simeq 998(\tau_i + \frac{1.25}{\tau_i}) \qquad (2.23)$$

where τ is measured in A.U., t_{ts} is in seconds and 998 is twice the conversion factor.

The spatial separation between the Orbiters and Landers is small, about 5 10^4 km at most, and the spatial separation between the thin screen points is even smaller. The velocity of the solar wind is about 400 km sec^{-1} at 1 A.U., which implies that the spatial separation between the thin-screen points introduce timing errors on the order of 2 minutes. With a plasma delay rate of 1 μsec/hour (a large value), these timing errors would introduce a plasma delay error of 35 nsec, which is not negligible. We found from numerical studies that our plasma estimates were remarkably insensitive to thin-screen errors on the order of an hour or less. It was decided to ignore the spatial separation between measurements and desired corrections for the present.

In two-way ranging, the spacecraft acts as a transponder. It receives the uplink ranging signal, and amplifies

and rebroadcasts it back to Earth. In order to avoid cross-talk between the transmitter and receiver on board the spacecraft, the transponder coherently multiplies the carrier frequency. The received frequency is multiplied by b (equal to 240/221) for the S-band downlink, and by k (equal to 880/221) for X-band. Using these turn-around ratios and Equation 2.19, the range measured at S-band is

$$\tau_s \simeq R_{up} + R_{down} + \frac{P_{up}}{f^2} + \frac{P_{down}}{(kf)^2} \qquad (2.24)$$

and at X-band is

$$\tau_x \simeq R_{up} + R_{down} + \frac{P_{up}}{f^2} + \frac{P_{down}}{(bf)^2} \qquad (2.25)$$

where R_{up} and R_{down} are the true uplink and downlink range, and frequency independent effects have been ignored.

Let SX_{delay} be equal to $(\tau_s - \tau_x)$, which can be found if τ_s and τ_x are measured. Thus,

$$SX_{delay} \simeq \frac{P_{down}}{f^2}\left(\frac{1}{b^2} - \frac{1}{k^2}\right) \qquad (2.26)$$

is an estimate of P_{down} only, as indicated earlier. The total S-band correction is

$$SXCOR = \frac{1}{f^2}\left(P_{up} + \frac{1}{b^2} P_{down}\right) \qquad (2.27)$$

In the static model, which assumes that $P_{up} = P_{down}$, Equation. 2.25 becomes

$$SXCOR = \frac{P_{down}}{f^2}(1 + \frac{1}{b^2}) = 2.3544\ SX_{range} \quad (2.28)$$

The standard convention is that the time tag associated with any range or Doppler measurement is the time of signal reception at the Earth. If $P_{down}(t)$ denotes the plasma delay contribution from P_2 at time t (which will influence the measurement on the ground at time $t + D_i$) then

$$SX_{delay}(t_i) = \frac{P_{down}(t_i - D_i)}{f^2}\ (\frac{k^2 - b^2}{k^2 b^2}) \quad (2.29)$$

If $SXCOR(t_i)$ refers to the S-band correction for a range measurement with time-tag t_i, then, from Equations 2.26 and 2.28

$$SXCOR(t_i) = \frac{1}{f^2}(P_{up}(t_i - (B_i + C_i + D_i)) + \frac{1}{f^2}P_{down}(t_i - D_i)) \quad (2.30)$$

Given an estimate of the thin-screen time, Δt_{ts}, and an estimate, $\hat{SX}(t)$, of the SX_{delay} then the estimate of SXCOR, $\hat{SXCOR}$ is

$$\hat{SXCOR}(t_i) = \frac{k^2}{k^2 - b^2}(\hat{SX}(t_i) + b^2\hat{SX}(t_i - \Delta t_{ts})) \quad (2.31a)$$

for an S-band delay correction. Using the numerical values for b and k, we get

$$\hat{SXCOR}(t_i) = 1.080357\ (\hat{SX}(t_i) + 1.179337\ \hat{SX}(t_i - t_s)) \quad (2.31b)$$

It might be wondered if the approximations used in Equation 2.18 are justified. I compared t_s calculated by Equation 2.32 with delays determined from an accurate ephemeris. This comparison is shown in Table I. The maximum timing error near superior conjunction is about 30 seconds. With a plasma delay rate of 1 μsec/hour (a large value), this timing error would cause a 9 nsec error in the plasma delay correction.

TABLE I

Date		t_s (seconds)		
MM/DD/YY	Julian Day	Accurate	Approximation	Error
11/04/76	2443087	1541	1507	34
11/14/76	2443102	1522	1501	21
11/27/76	2443110	1511	1497	14
12/09/76	2443122	1496	1488	8

From an ephemeris, the spatial separation between P_1 and P_2' can be calculated explicitly. It is planned to eventually take account of the spatial separation between P_1 and P_2' by multiplying the matched downlink delay by

$$\left(\frac{r(P_1)}{r(P_2')}\right)^{2.4}$$

where $r(P_i)$ is the Sun-P_i distance.

D. The Measurement Apparatus

Range and Doppler are measured at the stations of the Deep Space Tracking Network (DSN). The DSN maintains three

tracking station complexes, spaced so that any interplanetary spacecraft is visible from at least one of them at any time. One station at each complex is responsible for most of the dual-frequency radio tracking: DSN 14 at Goldstone, California, DSN 43 near Canberra, Australia, and DSN 63 near Madrid, Spain. Each of these is a fully steerable, azimuthally mounted, paraboloidal antenna 64 meters in diameter. The 26-meter diameter antenna at DSN 12, on Goldstone, California, has been used for SX measurements since mid-1978.

Since about 1970, range delay at the DSN has been measured by ranging machines which use a sequential ranging technique (reference 2-5). In sequential ranging, a square wave or sine wave sequence modulates the carrier before transmission, and the transmitted and received signals are correlated to estimate the range delay modulo the sine or square wave period. To resolve the delay ambiguity, the period of the modulation sequence is doubled and the correlation repeated, yielding the range modulo the longer period. This process is repeated until the codelength is larger than the a priori range uncertainty. Each sequence with a given period is said to determine a ranging code component.

The synthesizer frequency used, f_s, ($\sim$ 22 MHz) is multiplied by 96 to yield the transmitted carrier frequency, f_c, of 2.1 GHz. For the Planetary Ranging Assembly (PRA), which uses square wave modulation only, the transmitter range coder output has a period of

$$t_n = \frac{64 \cdot 2^n}{3f_s} = \frac{2^{n+11}}{f_c} \qquad (2.32)$$

where n, a positive integer, is called the order of the code component. Note that the transmitter code period is a function of the carrier frequency. The MU-2 machine, which can use sine wave modulation, can essentially operate with n equal to zero. It can be seen from a graph of the correlator outputs (Figure 3), that the correlation must be done in quadrature to completely resolve the range code phase.

Two types of ranging machines, the PRA (also called the PLanetary OPerational ranging machine, or PLOP) and the MU-2, are now used to make dual-frequency range and Doppler shift measurements. The MU-2 is an experimental ranging machine (only one exists) and is the only machine capable of making unambiguous SX range measurements. The PRA machine is the standard DSN ranging machine, and is used at every DSN station. From the start of the mission (1975) until April 15, 1977, the MU-2 machine was at DSN 14. From November 15, 1978 until mid 1979, this machine was at DSN 43. While the MU-2 was at DSN 14 it was used exclusively with square wave modulation, but after it was moved to DSN 43 it was used exclusively with sine wave modulation. (A. Zygielbaum, private communication).

The bandwidth of the spacecraft transponder is about 3.5 MHz, which, together with the choice of code component lengths (Equation 2.34), limits the smallest code component

to a period (or length) of 2 μsec for square wave modulation, and to half that for sine wave modulation. The measured range delay is discretized at the sub-nsec level, and has an experimental scatter of about 10 ns or less under good conditions (references 1, 4, 5). The carrier frequency Doppler shift is measured by a Phase Locked Loop (PLL) in the receiver which counts cycles of phase in the received signal using the transmitted signal as a phase reference. Figure 2 shows a block diagram of the S-band ranging system (after reference 3).

The PRA machine can correlate all of the range components of one (S-band or X-band) received range code. The other frequency code (usually chosen to be the X-band code) can only be correlated with the shortest (2 μsec) code component. Thus the PRA machine measure the S-X range modulo t_i, which is about 2 μsec (see Equation 2.34). This SX range ambiguity must be resolved by other means. The details of resolving the PRA SX ambiguity are discussed in the next chapter, in Section C.3.

The spacecraft will, in general, be in motion with respect to the ground station. A change in range during a range measurement causes a change in the phase of the returning modulation. To increase integration times, the carrier frequency shift is used to produce a corresponding change in the phase of the range correlation template.

E. Terrestrial Propagation Effects

The Earth's ionosphere, being a dispersive medium, also contributes to the measured plasma delay. Faraday rotation measurements of the ionospheric delay, which are available for each of the DSN stations, can be used to improve the plasma delay correction. The Faraday rotation from each tracking station to an Applications Technology Satellite in geosynchronous orbit is integrated continuously, sampled every 60 seconds and the resulting data are mapped to the spacecraft's direction by use of the thin shell model. In this model the ionosphere is assumed to be a shell of constant thickness and density at a constant height above a spherical Earth.

Let E(t) be the spacecraft elevation angle and $D_z(t)$ be an estimate of the zenith ionosphere delay, then the spacecraft ionospheric delay estimate is

$$\text{ION } E(t) = \frac{D_z(t)}{(1 - (r_1/r_2)^2 \cos^2 E)^{1/2}} \qquad (2.33)$$

where r_1 is the radius of the Earth, and r_2 is the mean radius of the ionospheric shell. If r_1 is assumed to be 6378 km and $r_2 - r_1$ is equal to 350 km, then $(r_1/r_2)^2$ is 0.89866, which is the value used at JPL. For each pass at each ground station, a fifth order polynomial, considered to be a function of time rather than E, is fitted to ION E(t) over the entire pass. These polynomials, prepared under the direction

of Dr. H. Royden at JPL, will be made available to MIT at some time in the future.

Each DSN station uses one satellite to measure the local ionospheric delay. In some cases, several satellites are visible from one station, and the ionospheric delay could be measured in several directions simultaneously. This additional data could be used to improve the mapped delays. It was concluded by Dr. Royden from comparison between mapped delays obtained from different ATS satellites that, for production polynomials, it is sufficient to use only one satellite per station (H. Royden, private communication).

Unfortunately, Faraday rotation measurements cannot measure the total plasma delay, only the change in the delay over an observing session. With geosynchronous satellites observing sessions last infefinitely, sometimes for many months, and are only interrupted due to equipment failures. Thus the Faraday rotation measurements contain a consistant unknown bias. An attempt was made to estimate the bias from consistency (the ionosphere delay must be positive at all times) and from comparison with ionosonde data, but it must be assumed that there is still a bias in the ionospheric zenith delay estimates on the order of the nighttime zenith delay, about 2 nsec at S-band. There is no reason to expect the bias to be the same at each station, which means that there probably would be systematic errors on the order of 2-5 nsec between polynomials from different stations. Note that

a bias in the zenith delay causes nonconstant error in the delay mapped to the spacecraft. Thus the bias will not, in general, be the same when comparing the ionospheric delay estimate from one station at different times.

The ionosphere data can be used to improve the interpretation of Lander delay measurements. First, Lander and Orbiter tracking data are often taken at different stations, and these stations do not share the same ionospheric contribution. The polynomials can thus be used to replace the contribution to the plasma delay from the Orbiter station ionosphere with that from the Lander station ionosphere.

Second the thin-screen model does not properly model the ionospheric delay contribution. The uplink ionospheric contribution is made at the uplink send time, some time before the matched downlink ionospheric contribution. The polynomials can be used to replace the receive time ionospheric contribution in the matched observable by the appropriate send time ionospheric delay. These corrections will be most important far from superior conjunction, when the solar plasma delay is small, and the ionosphere contributes a large fraction of the plasma delay.

The zenith ionosphere delay can be modeled by a rectified diurnal sine wave with a peak S-band zenith delay of about 10 nsec at local noon, and a fairly constant night-time value of about 2 nsec. At an elevation angle of 10°, the S-band ionospheric delay is therefore approximately 30 nsec.

Only differences in the ionosphere between the stations cause errors, however, and the ionospheric delay could be the dominant cause of error only for lander observations at low elevation angles.

The terrestrial atmosphere does not contribute to the SX observables, since the neutral atmosphere delay is independent of frequency. The atmospheric delay must therefore be estimated by other means. The atmopshere can also be treated by the slab model (Equation 2.33) in which r_2, the slab radius, is equal to r_1, the radius of the earth. This immediately gives a cosecant law mapping between the spacecraft atmopsheric delay and the zenith delay. The zenith delay, typically about 7 nsec at radio frequencies, is estimated from monthly averages of the pressure and humidity at the ground station. This correction is calculated in PEP and stored in CAL(1) (see Appendix III).

Data from both the Orbiters and the Landers are necessary for the general relativity experiment and for many studies of solar system dynamics. In this experiment, the Orbiters are used to estimate the plasma delay and the Landers are used to determine the motion of Mars. To use Orbiter plasma delay measurements to estimate Lander plasma delays requires an extrapolation across space and an interpolation in time.

The temporal separation between Lander and Orbiter SX measurements is not a negligible source of error. A scheme

for temporal extrapolations was devised after an investigation of the statistical properties of the plasma delay. This investigation is described in Chapter 4. Chapter 5 discusses the application of plasma delay interpolations to Lander range measurements. The next chapter discusses the computer processing required before use can be made of the SX delay and Doppler measurements.

Chapter III

Computer Data Processing

A. Introduction

Extensive computer processing is required before use can be made of the data collected at the tracking stations of the Deep Space Network (DSN). The observables wre described in Chapter II. Computer processing at JPL involves merging, editing, and reformatting the raw data tapes. The results are then copied and mailed to MIT, where the computer processing is completed. The processing done at MIT includes applying calibrations, merging, editing and reformatting the data.

This chapter is concerned with the processing of the Orbiter radio tracking data. First, I discuss the transferral of data from JPL to MIT and the problems of obtaining a complete data set. Second, I discuss the nature and type of the various range calibrations and the method of removing PRA SX range ambiguities. Finally, I describe the algorithms used in data editing.

B. Data Collection

Range and Doppler data were recorded at JPL on Project Tracking Tapes (PTT), which also contain engineering data from both the spacecraft and the ground station. At JPL the PTT are read and processed by the JPL Orbit Data Editor (ODE) program. The resulting ODE tapes, called ODFILES at JPL, are edited and used for orbit determination at JPL. Originally,

I used SX data obtained from copies of the ODE tapes mailed to MIT. A print-out of edited SX data used at JPL contained about 20% more data than were available from the MIT copies of the ODE tapes. Therefore, our computer programs were modified to process the PTT tapes sent to MIT in the hope that they would contain the missing data. This did not turn out to be the case. Each of the three data sets available at MIT (the PTT, the ODE tapes, and the JPL printout) contained good data not available on the other two. The missing data problem has never been satisfactorily resolved, but at least part of the problem seemed to be the use of different editing algorithms. The data used in this experiment consisted of data from all three sources. As can be seen in Table III, the ODE data not on the PTTs contributed about 20% of the SX data used.

In April, 1978, the PTT data format was superseded by the Archive Tracking Data File (ATDF). Figure 4 describes the data flow stream for the ATDF's. A variety of information must be transmitted from the ground station to JPL. Data types include range and Doppler data, spacecraft telemetry, itself from a variety of sources, and engineering telemetry from the ground station. Data at the ground station are blocked and formatted by the Metric Data Assembler (MDA). Each data block is sent to the star switch controller, which creates packets from the data blocks.

Packet switching is used since many sources send data intermittently, and in packet switching there is no need to pre-allocate data rates. This flexibility is obtained at the cost of some overhead, since each packet must contain the information (data source, time, etc.) needed to reconstruct the data stream at JPL.

The packets are transmitted over satellite data links to JPL, and are written onto the Network Data Logs (NDL). The Network Data Processor (NDP) is a program which separates the packets and reconstructs the data. The output from the NDP, the Intermediate Data Record (IDR) are kept for about two weeks at JPL. The ATDF tapes are designed, as the name indicates, for archival storage of the tracking data. The ODFILE's are created from the ATDF (or from the PTT) by a program at JPL called the Orbit Data Editor (ODE). The ODFILE's are used at JPL for orbit determination and the production of ephemerides, in much the same manner as the OBSLIB data type is used at MIT.

The processing up to the NDL resembles a data communication stream, and is designed to transmit data with a minimum of human intervention. The NDP is sometimes run several times on the NDL in case of suspected tape reading errors. The ATDF are supposed to contain all available data, without editing. The ATDF tapes have never been checked against the appropriate ODFILE data tapes to ensure that this missing data problem is solved.

The data tapes from JPL are not in a format convenient for use by the MIT data processing programs. Upon receipt of the PTT, ATDF or ODFILE tapes, the information within is reformatted for use at MIT. Lander tracking data is placed onto OBServation LIBrary (OBSLIB) data tapes. The format chosen to store Orbiter SX data is called the SXFILE, and is described in Appendix II. SX data are placed upon the SXFILE in time order. A program, SXDIFF, written by or Paul MacNeil of MIT, was used to remove S-band and X-band data from the PTT and to write an SXFILE containing the data. The program was later modified by Dr. MacNeil to process the ATDF format data as well. Another program, ODEPEP, is used at MIT to convert ODE tapes into the OBSLIB format which can be read by PEP. I modified a program, SX CALibration (SXCAL), written by Dr. Robert Goldstein (then with the Radio Science Group at MIT), to convert S-band and X-band data on OBSLIB tapes into the SXFILE format. In this way it was possible to use the dual-frequency data from the ODFILES.

The processing of Lander S-band range is conceptually very similar to Orbiter range data processing. In particular, the Lander range calibrations have the same format as the Orbiter range calibrations, and the computer subroutines that were written to apply the Orbiter calibrations have been adopted to apply Lander range calibrations. The Lander S-band data for this experiment were calibrated and edited by Dr. Goldstein. He put them onto OBSLIB tapes with the use of the programs ODEPEP and SXCAL.

C. Data Editing and Calibration

I wrote a number of programs to assist in processing the SX data, the most important of which were the Merge Fix and Edit (MFE) program and a pair of programs to list and plot the SX data: LISTSX and PLOTSX. The MFE program actually applies the range calibrations and deletes bad data, as well as merging SX data from several input SXFILE tapes. The LISTSX and PLOTSX programs are used to inspect the data, especially in connection with data editing.

There are four stages in the processing of raw SX range data. These four operations are, in order of use, the RANge CALibration (RANCAL) application, removal of the SX BIAS (SXBIAS), resolution of the 2 μsec PRA range ambiguity (called the PRA demod) and data editing. The Doppler data require no calibrations but do require extensive data editing.

These operations will be discussed below in their order of use, although this order is not always strictly observed. In particular, it is often necessary to iterate the various steps, especially the data editing.

1. Range Calibrations

Range measurements contain instrumental and station-geometry delays that must be estimated and removed. The RANCAL provide an estimate of this excess range. Each RANCAL is the sum of three components, called the DSS, the Space-Craft (S/C), and the Z-Correction (Z-Corr) delays. The DSS

and spacecraft delays are estimates of the delay in the ranging hardware at the station and on board the spacecraft, respectively. The Z-Corr delay is an estimate of the delay caused by the site geometry. Note that all three delays refer to round-trip delays.

The DSS delay is an estimate of the delay inside the ground station electronics. It is measured before and after each ranging pass by a device called the test translator (for the 64 meter diameter stations) or by a device called the Zero Delay Device (ZDD), which is a transponder mounted on the antenna surface. The ZDD is used only on the 26 meter diameter antennas. I will discuss only the test translator, since SX measurements are made mostly at the three 64 meter stations.

The test translator acts as a transponder at the front end of the ranging system. The test translator is a mixer which couples the transmitter klystron and the receiver front end (Figure 6). By mixing the transmitted signal with the appropriate intermediate frequency, it can simulate both the S- and the X-band turn-around ratios, and thus the S- and X-band calibrations are measured independently. The DSS delay shows a scatter due to measurement noise and due to occasional equipment changes, with the local standard deviation typically being about 5 nsec. The DSS measurements contain definite outliers, or bad measurements, which are typically many tens of standard deviations away from the

local mean. It was thus necessary to edit the RANCAL's. We chose to delete any point greater than 5 standard deviations away from the local mean. Figure 5 shows a plot of RANCAL's with deletions.

The spacecraft delay is an estimate of the transponder turnaround time and is calculated from telemetered spacecraft temperature and signal strength measurements. Before launch, the spacecraft delay was measured at a variety of internal spacecraft temperatures and these measurements were used to construct a calibration table of spacecraft temperature versus internal delay. During the mission, the spacecraft delay was calculated from telemetered temperature measurements by a table lookup and interpolation.

The Z-Corr calibration converts the range delay measured by the electronics to the delay that would have been measured if the ranging machine had been at the station reference location (see figure 6). The Z-Corr includes the propagation delay from the antenna aperture plane to the test translator, as well as τ_g, the delay between the antenna aperture plane and the site reference location, both of which are calculated from station geometry. The Z-Corr also includes the delay in the waveguide between the feedhorn and the test translator which is calculated, and the delay in the test translator itself which is measured. The Z-Corr delay estimate for any station is constant at the 0.1 nsec level throughout the mission. (The Z-Corr for the 26 meter stations must include the path length to the ZDD.)

The RANCAL's used in this experiment are prepared under the direction of Tom Komarec at JPL. The value of the calibration is punched onto cards, called the RANCAL cards, with one card per pass for each band. These cards are mailed to MIT where they are edited and stored on disk.

Dr. Goldstein and others at MIT wrote a subroutine package, USeR CALibrations (USRCAL), which finds the RANCAL for a particular pass, performs data conversions, and returns the calibration in seconds of delay scaled to the appropriate frequency. USRCAL is called once for each band for the dual-frequency data, and the SX calibration is formed from the differenced S-band and X-band calibrations. If no RANCAL exists for some pass, another RANCAL value is selected and used. From the set of all RANCAL's for the appropriate spacecraft, ground station and band, the selection algorithm selects the RANCAL from the pass closest in time to the target pass.

2. The SX Bias

Immediately after launch, when the spacecraft was still within a few million km of the Earth, the measured SX delay was negative. It was concluded by the spacecraft navigation team at JPL that this negative bias was caused by unmodeled systematic errors in the ranging system. The SX range measured during the early cruise phase was averaged, and this average was subtracted from all SX range measurements. The estimate of the bias in the SX range is called the SXBIAS.

The estimated SXBIAS is given in Table II (these values are added to SX delay). The cause of the SXBIAS is currently still unknown. The procedure followed in estimating the SXBIAS does not inspire confidence. The plasma delay contributions of the terrestrial ionosphere and plasmasphere were ignored in this averaging, so that there is an additional bias on the order of -10 nsec of SX range still in the SX data.

TABLE II

STATION		SXBIAS nsec
DSN 14	before JD 2443300	20
DSN 14	after JD 2443300	26
DSN 43		26
DSN 63		26

3. The PRA Demod

The PRA ranging machine can measure the SX range only to within modulo t_1, the period of the shortest PRA range component (about 2 μsec - see Chapter II.D and Equation 2.29). An appropriate integer multiple of t_1, determined from nearby MU-2 data, must be added to each PRA SX range, a process called "demodding" the PRA DATA. Demodding is reliable if the total SX delay can be estimated with an error much less than t_1 from nearby MU-2 SX measurements.

The difficulty of the PRA demod depends strongly upon time. Further than 20 to 30 days before or after superior conjunction, the total SX delay is less than 1 μsec and demodding is unnecessary. Within 2 to 3 days of superior conjunction, rapid plasma delay fluctuations make demodding unreliable.

PRA demod values are determined manually, typed onto cards, and input to the MFE program, which actually applies the demod. PRA SX range data are adjusted by multiples of t_1 until they match nearby MU-2 SX in both slope and level. If the demod value is not clear from the data, the PRA datum is deleted.

Lander delay residuals have a scatter of ∿100 nsec near superior conjunction. If the Lander plasma correction depends on PRA SX range data, the Lander range residual can be used to test the validity of the PRA demod. An error of t_1 in a Lander delay calibration is immediately detectable, which provides an independent check upon the validity of PRA demod values used in lander range calibrations (of course, we are especially interested in just those data).

D. Data Editing

Approximately 2 10^4 SX delay measurements and 5 10^5 SX Doppler shift measurements are available for this experiment. The sheer amount of data to be processed made data editing an important part of this experiment. The SX delay data were edited semi-automatically. The SX Doppler data would require

automatic or interactive data editing if more than a small subset of the data were to be used. The Doppler cycle slip problem considerably complicates automatic Doppler editing.

SX delay data editing was done iteratively. In the first editing pass, immediately after the PRA demod, the MFE program was used to delete all SX delay points in a data segment for which

$$SXMIN \leq SX_{range} \leq SXMAX$$

did not hold, in order to delete obviously bad data. Each data segment typically covered a month's worth of data. SXMIN and SXMAX were chosen, from a first look at the unprocessed data, to lie just outside of the range of reasonable results for the data segment being processed. For example, near superior conjunction, SXMIN = -100 nsec and SXMAX = +100 μsec were used.

After the first pass of data editing, the data were reviewed and edited manually, with the help of the LISTSX and PLOTSX programs. Delete cards (which specify a span of data to be deleted) were then prepared for input to the MFE program, which actually deleted the data.

Table III gives a summary of the data editing process. 4070 SX delay measurements (or 19%) of the total 21924 SX delay measurements were deleted. Of the 4070 deletions, 636 (or 16%) came from the delete on SXRMIN and SXRMAX and the rest were manual deletions.

Table III

SX Delay Data Sources

JD 2442950 - 2443434

Spacecraft	PTT Data	ODE Data	On ODE but not PTT	Total Data	Total Deletions	Total Good Points
VO1	9083	9905	1199	10282	--	--
VO2	9391	10560	2251	11642	--	--
Total	18474	20465	3450	21924	4070	17854
JPL print-out data						227
Grand Total						18081

Two categories of bad SX delay data can be distinguished, isolated bad data and groups of bad data. Within a bad data group, the SX delay estimate are typically scattered between SXMIN and SXMAX, with no apparent correlation between adjacent measurements. All observations within a bad data group were deleted, not just the points away from the local mean (Figure 8). Bad data groups typically, but not always, occur at the beginning or end of a pass. It is known that the ranging system collected "data" at times when the spacecraft was not above the local horizon. At least some of the

bad data groups can be attributed to this cause. Other bad data groups are caused by equipment problems at the tracking station (A. Zygielbaum, personal communication).

An isolated bad datum (Figure 9) is one bad point in the midst of a good data sequence. The cause of such bad data is unclear. For isolated bad data, the local standard deviation was estimated and the point deleted if it was more than 5 standard deviations from the local mean. Isolated bad data are hard to catch by eye, and this stage of the data editing was iterated several times. It might be possible to automate the deletion of isolated bad data in the future.

The SX Doppler data could be used to improve Lander plasma delay estimates. Data editing problems have prevented this for this experiment. The Doppler data suffer from cycle slips, which are phase errors of a multiple of 1 cycle of phase in the Doppler phase counting. Uplink phase noise is included in the multiplication up to X-band at the spacecraft, which reduces the signal-to-noise of the signal received on the ground. At times of rapid spacecraft acceleration (such as near periapse) the X-band Doppler phase changes too fast for the Doppler cycle counter at the ground station to maintain lock.

For SX Doppler editing it is necessary to be able to reliably detect cycle slips in the data. Near superior conjunction, the scatter in the Doppler data masks possible cycle slips. Figures 10 and 11 illustrate the problem. Two

overlapping integrated Doppler sequences from different spacecraft are compared. Figure 10 shows the overlapping data, which diverge due to cycle slips at about $23^{hr}\ 40^{min}$. It would be impossible to reliably detect these cycle slips without overlapping Doppler data. Figure 11 shows the overlapping data after the removal of the cycle slips.

After processing, the Orbiter SX data must be applied to Lander range data. Chapter IV describes the statistical nature of the plasma delay, and Chapter V the application of the plasma data to the Lander observable.

Chapter IV

The Statistical Nature of the Plasma Delay

A. Introduction

As was shown in Chapter II, the solar plasma contributes to the measurements of the delay and Doppler shift made with the Viking spacecraft. To make full use of these measurements, it is necessary to estimate and remove the plasma delay contribution to the measured delay to the Lander.

The plasma density in the solar corona is subject to wild fluctuations (reference 8) and is beyond our capabilities to model adequately from first principles. In such circumstances it is natural to consider statistical models of the plasma delay. It was decided to ignore the spatial separation between measurements, and to treat the SX plasma measurements as a function of time only.

In this chapter, I will discuss a statistical study of the SX plasma measurements. I will define the autocorrelation of a random sequence, and will describe the results of autocorrelations of the SX data. Given the available data, I conclude that the appropriate model of the plasma delay is a random walk. I will then discuss the implications of that conclusion for plasma delay estimation. In the next chapter I will discuss results obtained from applying these conclusions to the estimation of plasma delay corrections from the Lander S-band delay measurements.

B. The Plasma Autocorrelation

A random process, x_t, is called weakly (or wide sense) stationary (reference 19, pp 55-56) if it has a time invariant probability density function, and if

$$c(\tau) \equiv \text{Expectation } (x_t x_{t+\tau}) = \langle x_t x_{t+\tau} \rangle \quad (4.1)$$

exists and is a function of τ only. In this case, the function $c(\tau)$ is called the autocovariance function of x_t, and

$$\rho(\tau) = \frac{c(\tau)}{c(0)} \quad (4.2)$$

is the autocorrelation function (ACF) of x(t).

Let x(t) be a zero mean, weakly stationary, random process, sampled at equal intervals Δt for N observations starting at time t_o. (Thus, the observation times are t_o, $t_o + \Delta t$, ..., $t_o + (N-1)\Delta t$.) An unbiased (but not necessarily minimum variance) estimator for $c(n\Delta t)$, $\hat{c}(n\Delta t)$ is:

$$\hat{c}(n\Delta t) = \frac{1}{N-n} \sum_{i=0}^{N-n} x_{t_o+i\Delta t}\, x_{t_o+(i+n)\Delta t} \quad (4.3)$$

This estimator is not generally unbiased for nonstationary processes; indeed, the autocovariance as defined above may not even exist for nonstationary random processes.

The epochs of the plasma delay and delay-rate measurements are not in general evenly spaced and thus Equation 4.3 cannot be used directly. The standard modification of Equation 4.3 for unevenly spaced data is

$$\hat{c}(n\Delta t) = \frac{1}{N(n)} \sum_{\substack{\text{all pairs} \\ \text{with } t_1 \leq t_2}} x_{t_1} \cdot x_{t_2} \cdot w(n, t_2 - t_1); \quad n > 0 \qquad (4.4a)$$

with

$$N(n) = \sum_{\substack{\text{all pairs} \\ \text{with } t_1 \leq t_2}} w(n, t_2 - t_1) \qquad (4.4b)$$

and

$$w(n, t_2 - t_1) = \begin{cases} 0 & t_2 - t_1 < (n - 1/2)\Delta t \\ 1 & (n-1/2)\Delta t \leq t_2 - t_1 < (n+1/2)\Delta t \\ 0 & (n + 1/2)\Delta t \leq t_2 - t_1 \end{cases} \qquad (4.4c)$$

In Equations (4.4a) and (4.4b), "all pairs with $t_1 \leq t_2$" really mean all pairs of observations at times t_1, t_2 for which $t_{start} \leq t_1 \leq t_2 \leq t_{finish}$ where $t_{finish} - t_{start}$ is called the integration time. This extension to Equation 4.3 is due to Parzen, see reference 24. I wrote a computer program, the Plasma Autocorrelation Program (PAP), to implement this algorithm.

1. The Autocorrelation of the SX Delay

The plasma delay is not weakly stationary, as neither its mean nor its variance are constant with respect to time. (See Figure 12 for SX plasma delay measurements taken near superior conjunction.) The long-term trend in the plasma delay makes it non-stationary over time spans much longer than a day. This non-stationarity must be removed before PAP can give meaningful autocorrelation estimates for lags on the

order of a tenth of a day or more. The primary cause of nonstationarity in the SX delay measurements is the changing raypath geometry. We hypothesized that this nonstationarity could be removed by normalizing the integrated plasma density with a geometrical correction factor, obtained by integrating a static plasma density model over each ray path.

A simple, commonly used model of the plasma density is (reference 20):

$$\rho(r) = \rho_o\left(\frac{r}{r_o}\right)^{-n} \quad \text{in electrons cm}^{-3} \qquad (4.5)$$

Here r is the distance from the Sun, in units of the solar radius, R_0 and r_o is generally taken to be 1 A.U. or $\backsim 215\ R_0$. Numerous studies have shown that $n \backsim 2.4$ and $\rho \backsim 7.5$ electrons cm^{-3} best fit the coronal plasma density at $r \quad 5R_0$. The density integrated over the raypath given in Chapter II is

$$H(\ell) = \int_{\text{Earth}}^{\text{Mars}} \rho(r)dx \qquad (4.6)$$

where ℓ is the raypath impact parameter.

It is useful to assume that the measured SX delay is a function of a stationary random process, SX', and a deterministic function such as $H(\ell)$. If the SX delay was an additive function of SX' and $H(\ell)$, SX' could not be stationary, since the variance of the SX delay fluctuations increases

near superior conjunction. We hypothesized that the SX delay was a multiplicative function of SX' and H(ℓ), or that

$$SX' = SX/H(\ell) \qquad (4.7)$$

is the assumed stationary process.

From an analysis of the Viking Orbiter SX delay measurements I found that

(A) SX varied from 10 nsec to 50 μsec over the region of observations, or by over 3 orders of magnitude. The local variance was roughly proportional to the mean.

(B) SX' varied from 0.2 to 1.6 over the same period, with the local variances being roughly constant with time. SX' varied over less than 1 order of magnitude.

(C) There is still a long-term trend near superior conjunction, but the normalized data come much closer to stationarity than do the unnormalized data. As an illustration, I will compare SX and SX' some 2 days before superior conjunction. Figure 13 is a plot of SX vs time and Figure 14 is a plot of the corresponding SX' vs time. Let SX be the average of the SX ranges shown in Figure 13, and let ΔSX be the peak-to-peak variation in Figure 13, then ΔSX/SX = 0.14. In an analogous way we

constructed $\Delta SX'$ and found that $\Delta SX'/SX' = 0.05$. The trend still visible in SX' might be due to local plasma fluctuations or simply to the inadequacy of the model, which does not take into account higher order terms in r, as in Equation 2.21. With the long-term trend partly removed, long arc autocorrelations of the SX delay could be obtained. They appear to show that the detrended SX range behaves as a random walk (see Figure 15). For a random walk the ACF decreases linearly with increasing lag, and the ACF of the first differences of SX delay measurements looks like uncorrelated (or white) noise (Figure 16).

2. The Autocorrelation of the SX Doppler

Continuity implies that the first difference of x_{t_i} must become correlated as $t_{i+1} \rightarrow t_i$. The Doppler shift is measured more often than the range, and thus provides a probe of higher frequency plasma fluctuations. The SX Doppler shift measurements should also be more accurate than the SX delay measurements.

Figure 17 is a plot of SX delay and integrated Doppler vs time some 16 days after superior conjunction. Notice that the delay and integrated Doppler agree on the 20 nsec level and that the Doppler sampling rate is 20 times that of the range. With this in mind, ACF's of the Doppler (which correspond to ACF's of the range differences) were obtained

(Figure 18). The average and the root mean square of the SX Doppler data sequences used in Figure 18 are shown in Table IV, the average of each SX Doppler data sequence is less than the corresponding rms in all cases, which supports the hypothesis that the SX Doppler are a zero mean random process.

TABLE IV

Statistics of SX Doppler Data Used in Autocorrelation Study

Spacecraft	t_1, Julian Date	t_2, Julian Date	Number of Observations	Average of Doppler Data, Hz	RMS of SX Doppler Data, Hz
VO2	2443095.353	2443095.595	349	-0.000491	0.1397
VO2	2443101.080	2443101.347	383	-0.2927	0.3516
VO2	2443117.685	2443117.800	166	0.0209	0.10587
VO1	2443124.839	2443124.9577	177	-0.00135	0.19388
VO1	2443160.885	2443161.317	606	0.00281	0.00937

Since the epochs of this data are equispaced, the ACF estimate provided by Equation 4.4 is identical to that in Equation 4.3, whose statistical properties are much better known. In particular, the standard deviation, σ, of estimates of the values of the ACF of a white noise process provided by Equation 4.3 is known to be approximately equal to $1/\sqrt{N}$, where N is the number of observations included in the estimate. (This estimate of σ is due to Bartlett, see reference 14, pp. 34-36). Lines at the 5σ level have been included with the plots of the Doppler ACF. Several of the

sample ACF's (in particular Figures 19a and c) show significant correlations at this level. The nature of the sample ACF's, with an apparently exponential decay with increasing lag in Figures 19a and e, and possible damped oscillations in Figures 19b, c, and d, suggest that the SX Doppler data may be best modeled as a low order Autoregressive (AR) process. An AR(n) process can be modeled by an nth order stochastic difference equation of the form

$$x_{t_i} = \sum_{k=1}^{n} \phi_K y_{t_{i-k}} + \beta_{t_i} \qquad (4.8)$$

where β_{t_i} is zero mean white noise sequence (reference 14, chapter III). x_{t_i} can be expanded in terms of a linear combination of past β_{t_i}.

Since the β_{t_i} are zero mean, x_{t_i} is a zero mean random sequence. If both sides of Equation 4.8 are multiplied by $x_{t_{i-m}}$, for m = 1,n and if the expected value is then taken and the resulting equations normalized by dividing by c(0), the so-called Yule Walker or Normal Equations result

$$\rho_m = \sum_{k=1} \phi_k \rho_{m-k} \quad m = 1, n \qquad (4.9)$$

These equations can be solved to give ϕ_k in terms of ρ_m. Estimates for the model parameters, $\hat{\phi}_i$, can be obtained from estimates of the ρ_i. The $\hat{\phi}_i$ obtained in this manner are not necessarily the best estimate of ϕ_i, since the Yule Walker Equations ignore possible errors in $\hat{\rho}$, but solutions to the Yule Walker equations are frequently used as a guide in model

identification. From the rapid decay of the SX Doppler ACF value with increasing lag, only low order AR models are suitable.

For an AR(1) process, Equation 4.8 reduces to

$$x_{t_i} = \phi_1 x_{t_{i+1}} + \beta_{t_i} \qquad \phi < 1 \text{ for stationarity} \qquad (4.10a)$$

the ACF decays exponentially

$$\rho_k = |\phi_1|^k \qquad (4.10b)$$

and the Yule Walker Equations become the trivial

$$\rho_1 = \phi_1 \qquad (4.10c)$$

An AR(1) process can be interpreted as samples of a first order Markov process

$$\frac{dx}{dt} = \frac{1}{\gamma} x(t) + \beta(t) \qquad (4.11)$$

Under this interpretation, Equation 4.10 becomes

$$x_{t_i} = c^{-\Delta t/\gamma} x_{t_{i-1}} + \beta_{t_i} \qquad (4.12)$$

and γ can be identified with the correlation or "1/e" time of an AR(1) process. Since Δt is known, γ can be estimated by

$$\hat{\gamma} = -\Delta t / \ln \hat{\phi}_1 = -\Delta t / \ln \rho_1 \qquad (4.13)$$

In testing a suspected AR(1) process, the null hypothesis is a white noise process. Under that, the estimate of the standard deviation of $\hat{\phi}_1$, σ_{ϕ_1}, is just $1/\sqrt{N}$.

The results of the analysis of the selected SX Doppler data is shown in Table V. At least two sequences have sta-

tistically significant values for ϕ_1. The Correlation times are all very short though, on the order of a minute or less.

The short correlation times of the SX Doppler imply that the Doppler and delay rate can be adequately modeled as a random walk. The SX delay is typically measured every four to eight minutes. The histogram of the number of Lander delay observations versus the time to the nearest SX delay measurement (Figure 21b) shows that 82.4% of all (usable) Lander delay measurements are further than 58 minutes from the nearest SX delay measurement. The SX Doppler data are uncorrelated over invervals of longer than a few minutes. As a practical matter, therefore, the SX delay data can be modeled as the integral of a white noise process, or as a random walk:

Table V

Parameter Estimates for SX Doppler Data

Time JD-2440000	N	σ_{ϕ_1}	$\hat{\phi}_1$	Fract $\hat{\phi}/\sigma_{\phi_1}$	$\hat{\gamma}$ min.
3095.353	349	.054	.599	11.2	1.95
3101.080	383	.051	.286	5.60	0.80
3117.685	166	.078	.199	2.56	0.62
3124.837	171	.076	.210	2.74	0.64
3160.885	606	.041	.310	7.63	0.85

The estimation of SX delays could be improved by using integrated Doppler to extend range sequences. The Doppler data, however, contain cycle slips (errors that are integral multiples of one cycle of Doppler phase at the ground sta-

tion), especially when the Doppler phase counter is highly stressed (i.e., when the Doppler rate is high). As there are about 10^6 SX Doppler observations, Doppler validation is a critical problem, one that I have chosen not to tackle so far (see Chapter III.D).

C. Estimation and Smoothing of a Random Walk Process

A random walk can be modeled by a stochastic differential equation:

$$\frac{dx}{dt} = w(t) \qquad (4.14a)$$

where w(t) is a white noise or Wiener process. An exponentially correlated random variable has an additional "feed back" term linear in X(t) on the right hand side. The equivalent discrete version of Equation 4.10a is

$$x_{t_i} = x_{t_{i-1}} + \beta_{t_i} \qquad (4.14b)$$

where the t_i are assumed equally spaced and β_{t_i} is a zero mean white noise sequence, assumed to have a symmetric unimodal distribution and a variance of σ_β^2 and a variance of σ_β^2. In that case x_{t_i} unimodal symmetrical distribution. The first difference of a random walk is

$$\nabla x_{t_i} \equiv x_{t_i} - x_{t_{i-1}} = \beta_{t_i} \qquad (4.11)$$

A random walk can be written as a sum

$$x_{t_i} = x_{t_{i-k}} + \sum_{\ell=0}^{k-1} \beta_{t_{i-\ell}} \tag{4.12}$$

The Maximum Likelihood Estimate (MLE) of a random variable with a symmetric unimodal distribution is the conditional mean of the variable, which is also the Minimum Mean Square Error (MMSE) estimate (reference 19, p. 149, pp.156-157). Under these assumptions, the MLE of the present state, x_{t_i}, given knowledge of some past state, $x_{t_{i-k}}$, is

$$\langle x_{t_i} | x_{t_{i-k}} \rangle = \langle x_{t_{i-k}} + \sum \beta_{t_{i-\ell}}^{k-1} \rangle = x_{t_{i-k}} \tag{4.13}$$

this is called the forward state estimate. The mean square error is

$$\sigma_f^2 = \langle (x_{t_i} - x_{t_i} | x_{t_{i-k}})^2 \rangle = \Delta t_f \sigma_\beta^2 = \sigma_f^2 \tag{4.14}$$

where Δt_f is $(t_i - t_{i-k})$ and is called the forward interpolation time.

In a similar fashion the MLE of x_{t_i} given knowledge of some future state, $x_{t_{i+m}}$, is

$$\langle x_{t_i} | x_{t_{i+m}} \rangle = \hat{x}_{t_{i+m}} \tag{4.15}$$

This is called the backward state estimate and the expectation of the mean square error is

$$\sigma_b^2 = \Delta t_b^2 \sigma_\beta^2 \qquad (4.16)$$

where Δt_b is $t_{i+m} - t_i$ and is called the backward interpolation time.

The optimal linear (MMSE) smoother is the weighted average of
the two estimates of x_{t_i} (reference 15, chapter 5):

$$\hat{x}_{t_i} = \frac{1}{\frac{1}{\sigma_f^2} + \frac{1}{\sigma_b^2}} \frac{x_{t_i}|x_{t_{i-k}}}{\sigma_f^2} \cdot \frac{x_{t_i}|x_{t_{i+m}}}{\sigma_b^2} \qquad (4.17)$$

Using Equations 4.14 and 4.16, the optimal linear smoother for a random walk process can be simplified to obtained

$$\hat{x}_{t_i} = p x_{t_{i-k}} + (1-p) x_{t_{i+m}} \qquad (4.18)$$

where p is $\Delta t_b/(\Delta t_f + \Delta t_b)$. The optimal linear smoother for a random walk is thus just a linear interpolation between the nearest data before and after the smoothed point.

Given a model of the plasma behavior, and an estimator based upon the model, it is possible to calculate plasma corrections. In the next chapter, I will discuss the application of plasma delay measurements to the Lander range

corrections, and the results of that application. The linear smoother derived in this chapter will be compared to other estimators.

Chapter V

Lander Plasma Corrections

A. Introduction

In the previous Chapter, I derived the optimal linear smoother for the SX delay data. Most of the processing required to calculate Lander plasma corrections is independent of the estimator used, and it was decided to write a program which could realize several estimators. In this way, it was possible to compare estimators from their effects on Lander delay residuals.

The first part of this chapter, I will describe the processing necessary to convert Orbiter SX range measurements into Lander plasma corrections. In the second part of this chapter, I will report the results of multiple parameter solutions using the Lander delay data, and finally the behavior of the postfit Lander residuals is explored.

B. Computer Processing of Plasma Corrections

As a means of applying plasma corrections to the Lander observations, I wrote a program, UPOLT (UPdate Observation Library Tapes) which reads an OBServation LIBrary (OBSLIB) tape and writes a new OBSLIB tape with the needed corrections stored on it. UPOLT was designed to provide flexibility in converting SX range measurements into Lander plasma delay corrections, and to serve as a framework for better interpolators as they were found. UPOLT performs the following functions:

A. Read in an OBSLIB tape and an SXFILE.

B. For each Lander range measurement, two subsets of the SX data are selected: One for the downlink and one for the uplink.

C. Various linear fits are made to each of the selected sets of SX data.

D. The Lander correction is the sum of the uplink and downlink correction, each of which is a weighted average of the linear fits to the data.

Each of these functions is described more fully below.

A. Part of the input SXFILE is read and used to fill a buffer containing the time of each observation and the measured SX delay. Then the OBSLIB tape is scanned sequentially. As needed, the buffer is filled with later SX information or the SXFILE tape can be rewound and the buffer refilled. This last option is needed as the OBSLIB tape does not contain observations in time order.

The time tag for any Lander delay observation is not necessarily the time for which the plasma delay estimate is desired. The measured Lander delay is the sum of the propagation delay over both uplink and downlink. The SX data are downlink only. Thus, each Lander range correction is the sum of two SX interpolations, one corresponding to the uplink and one corresponding to the downlink part of the signal. We are using the so-called "thin-screen" model, which assumes that the entire plasma effect occurs at the point where the ray

path passes closest to the sun (Chapter II C and reference 4). The thin screen is probably a good assumption near superior conjunction, where the plasma density increases as a high power of the distance to the sun. Far from superior conjunction, it may not be a good assumption, but there the effect of timing errors is much decreased. (Only near superior conjunction does the plasma show a rapid time variation.)

Both the SX delay time tag and the Lander delay time tag are the time of reception or, more precisely, the time of the start of the range correlation. As discussed in Chapter II, the downlink thin-screen time for a Lander delay calibration is just the Lander delay reception time, and the uplink thin screen time is the reception time minus the round-trip propagation time between Mars and the thin screen point. It would be possible to improve the thin-screen delay approximation given in Chapter II. However, numerical experiments show that plasma delay estimates are remarkably insensitive to timing errors on the order of many tens of minutes. In particular, an error of several hundred seconds in Δt_{ts}, detected after run AP-43C, causes negligible changes in the residuals. It is doubtful that much would be gained by using more accurate thin-screen times.

B. For each of the two thin-screen times, the following SX data were selected.

1. The two nearest SX points (before and after the thin-screen time) were found.
2. All SX points within a certain ΔT, called SPAN, of those two points were used.

C. A linear fit was made to three data sets chosen from the selected data. Each linear fit is a (non-weighted) least squares fit of a straight line to the selected data. The data sets fit to are:

1. All selected SX data before the epoch of the Lander observation.
2. All selected SX data after the epoch of the Lander observation.
3. All selected SX data.

D. The plasma delay estimate is obtained by combination of the three separate estimates by means of a weighted average

$$\hat{SX} = \sum_{i=1}^{3} SX_i/w_i^2 \sum_{i=1}^{3} \left[1/w_i^2\right]^{-1} \qquad (5.1)$$

In Equation 5.1, SX_i is the value of the SX from the ith fit, and $\hat{SX}$ is the interpolated SX value. The weighting scheme used was

$$w_i^2 = \begin{cases} c_i(\sigma_i^2 + \alpha|t_n - t_{ts}|) & i = 1,2) \\ c_i\sigma_i^2 & i = 3 \end{cases} \qquad (5.2)$$

where w_i is the weight given to the ith fit, σ_i is the formal error from the linear regression, t_n is the time of the SX datum that was nearest in time to t_{ts} and in the ith data set (see above), and the c_i and α are constants. t_{ts} is the thin screen time for the current Lander range observation (see Equation 2.23). In the standard parameter set, $c_1 = 1$, $c_2 = 1$, $c_3 = 0.1$, and $\alpha = 0.25 \times 10^{-12}$ (seconds of range)^2/day^2. The value of SPAN in the standard parameter set was 1 hour 12 minutes. Our working hypothesis was that SPAN should be set to the correlation time of the plasma measurements. One hour was the initial guess of this correlation time and SPAN equal to 0.05 day, or 1.2 hours, was the value chosen for the standard parameter set. As it turns out, <1 minute would be a more appropriate choice of ΔT.

Given SX for each of the two thin screen times, the Lander plasma correction at S-band (SXCOR) is given by

$$SXCOR(t) = \left(\hat{SX}(t) + b^2 \hat{SX}(t-\Delta t_{ts}) \right) k^2/(k^2-b^2) \quad (5.3)$$

where k is the X-band turnaround ratio, and b is the S-band turnaround ratio (see Equation 2.31a).

C. Lander Residuals and the Plasma Corrections

Lander residuals provide an independent test of our model of the plasma correction, which is not usually available in time series analysis. Residuals are defined by

$$r(t) = O(t) - C(t,\underline{\hat{y}}) \qquad (5.4)$$

where

$O(t)$ = the measured roundtrip range to the lander.

$C(t,\underline{\hat{y}})$ = the computed value of the observation given the parameter set $\underline{\hat{y}}$.

$\underline{\hat{y}}$ = the best available estimate of the true parameter set vector $\underline{y}$.

t = the time of reception of the lander range measurement.

The residuals are computed by the Planetary Ephemerides Program (PEP), which is described elsewhere (reference 18). PEP can calculate the theoretical observable and the partial derivatives of the observable to selected parameters from a parameterized model of motions of bodies in the solar system. PEP can use the resulting residuals, together with the partials, to do a least-squares solution for the parameter value. The partials, once calculated, can be stored on the OBSLIB tape with the observables, thus reducing the cost of each parameter solution.

In the work reported in this chapter, PEP was used to fit a model of the motion of the earth and Mars to the Lander delay data, and the sensitivity of the resulting postfit residuals was investigated. The model of the motion of the earth and the location of the ground stations were obtained

from previous optical and radio observations. The model of the rotation of Mars is described in reference 17.

In a standard parameter solution (these parameters must be distinguished from the UPOLT parameters) a 26-parameter model of the solar system is fit to the observations. The parameters used were: six initial conditions each for the orbits of teh earth and Mars, the mass of Mercury, Jupiter and the Moon, the rotation phase of the earth, the period of rotation and the direction of the axis of rotation of Mars, all at a given epoch, the coordinates of the Landers on Mars (three each) and the value of the astronomical unit in light-seconds. On some additional runs the relativity parameter "RELDEL" was also solved for.

In PEP, postfit residuals are predicted from the parameter adjustments and the partial derivatives of the observables with respect to the parameters. This is considerably cheaper than reintegrating the equations of motion using the new parameter values.

An estimate of the Lander plasma correction, SXCOR, is provided by the UPOLT program. The residual and computed lander range are updated with the new plasma corrections as is described in Appendix III.

We are driven to consider the lander residuals by two facts:

A. PEP uses a Weighted Least Squares Estimator to find $\hat{\underline{y}}$. The optimum weight for each observation is the

error associated with the observation. Appropriate weights can best be determined by a consideration of the residual scatter.

B. The residuals provide an independent check on the validity of the plasma model. Given any plasma model, we can derive the sensitivity of the plasma estimate to external conditions. By actually finding the sensitivity of the residual scatter to the same external conditions, a check of the validity of the plasma model can be made.

I wrote a program, the HistOGram (HOG) program, to

1. Group the residuals by external conditions.
2. Find the rms scatter within each group.
3. Plot the rms spread of the residuals vs the external conditions.

Even a cursory glance at a plot of lander range residuals versus time shows an increase in the residual scatter near superior conjunction (Figure 19). Thus the sensitivity of the Lander delay residuals to the temporal separation between the measurement time and the time of superior conjunction was investigated. Let

$$\delta T_{sc} = |T - T_{sc}| \qquad (5.6)$$

T = time of range measurement, in Julian days

T_{sc} = time of superior conjunction, T_{sc} = (244)3108.

HOG was run with all residuals for which

$$n\Delta t < \delta T_{sc} < (n + 1)\Delta t \qquad (5.7)$$

were grouped together where Δt is the bin size. The results are shown in Figure 20, which was used in deriving a formal error (σ) for each observation. The formal errors used were

$$\sigma(\delta T_{sc}) = \begin{cases} 20 \text{ nsec}; & |\delta T_{sc}| \geq 200 \text{ days} \\ (60 - 0.2 \cdot \delta T_{sc}) \text{nsec}; & |\delta T_{sc}| < 200 \text{ days} \end{cases} \qquad (5.8)$$

This corresponds to the heavy black line on Figure 20. These sigmas were chosen to make the root mean square (rms) of the weighted residuals be $\sim$ 1. They were used in a new weighted least squares parameter estimate in PEP, and caused only slight changes in postfit parameter estimates. With the new sigmas, the rms of the weighted were equal to .9727 for one solution (Appendix 1, Run AP-41R).

From now on, we will consider the weighted residual (residual/σ). An attempt was made to find the sensitivity of the weighted residuals on external conditions. It was thought possible that the weighted residuals might show a dependence upon the interpolation time of the estimate (i.e., the time from the lander range observation to the nearest SX range point), or upon the number of SX range points used in the fit, or upon the statistical error associated with the fit (which is a measure of how well the SX data agree with

the curve fit to them). HOG was run to investigate each of these three possibilities, and the results are shown in Figures 21, 22, and 23. Note that the rms of the residuals now center about 1.0, as weighted residuals were used. There is no apparent relationship between the weighted residuals and the other parameters. This can be explained by the random walk model as follows.

For a random walk, the nearest SX point contains all of the information available for extrapolation. In reality, there is random measurement noise associated with each range measurement. From data far from superior conjunction, it seems that this measurement noise has an rms of $\sim$20 nsec (Figure 19 and 20). Near superior conjunction this measurement noise is probably swamped by the plasma delay interpolation error. In this case, the estimate of the Lander plasma delay is not improved by including more SX points. Far from superior conjunction, this condition might not be valid.

The autocorrelation of SX range decreases very slowly with increasing lag (Figure 17). Thus, over times of the order of one tenth of a day, the extrapolation will be insensitive to the interpolation time (or to the statistical error, which is dominated by terms containing the interpolation time). One might expect that if the gap between SX observations and lander points was on the order of several days that some relationship could then be detected. We could easily test this by deliberately deleting SX data.

D. Experimental Tests of Our Conclusions

We have hypothesized that the random walk is a suitable model for the SX plasma delays. Under the random walk hypothesis the total information content of a sequence of plasma measurement is contained in the last measurement. Thus, all of the information available for interpolation is contained in the two plasma values immediately before and after the thin screen time. From this, two further hypotheses can be derived:

1. Any linear plasma delay estimator that includes a contribution from extrapolated plasma delay rates will have a larger mean square error than the optimal linear smoother and the more it relies upon the extrapolated slopes, the larger will be the mean square error.
2. The plasma delay interpolation should be insensitive to the number of SX data points used (see Equation 4.23).

Now, if C_3 is set to ∞ (in practice, 10^6), the plasma delay estimate will include a contribution from the extrapolated slopes. We hypothesized that this should be an unreliable plasma interpolator. We found that

$$\text{RMS } \frac{O - C}{\text{error}} = \begin{cases} 1.2 \text{ using } C_1=1,\ C_2=1,\ C_3=0.1 \text{ (AP-48F)} \\ 5.3 \text{ using } C_1=1,\ C_2=1,\ C_3=10^6 \text{ (AP-48E)} \end{cases} \quad (5.9)$$

with SPAN = 0.05 day.

This large increase in the rms error supports our hypothesis.

If SPAN is set to less than the time interval between measurements, then only two measurements, one before and one after, will be selected for use in the plasma delay estimate. If, in addition, $c_1 = 10^5$, $C_2 = 10^6$, $C_3 = 1$ or $C_1 = 1$, $C_2 = 1$, $C_3 = 10^6$ is used, then the estimate lies upon the straight line through the 2 data points. This corresponds to the optimal linear smoother for a random walk derived in Equation 4.18. Using these parameter values, we found that

$$\text{RMS } \frac{O - C}{\text{error}} = \begin{cases} 1.2 \text{ using SPAN} = 0.05 \text{ day (AP-48F)} \\ \qquad\qquad C_1 = 1.0 \\ \qquad\qquad C_2 = 1.0 \\ \qquad\qquad C_3 = 0.1 \\ \\ 1.0 \text{ using SPAN} = 1 \text{ minute (AP-48C)} \\ \qquad\qquad C_1 = 1.0 \\ \qquad\qquad C_2 = 1.0 \\ \qquad\qquad C_3 = 10^6 \end{cases} \tag{5.10}$$

Run AP-48F is a standard parameter set run, which uses about 20 SX data points for each Lander plasma delay calibration, and for which the plasma delay estimate is a weighted sum of three linear fits to the selected SX data, as in Equation 4.22 and 4.24. Run AP-48C implements the optimal linear smoother of Chapter IV, which uses only two SX measurements per plasma delay estimate. This does as well as the much more complicated smoother implemented in the first run. Under the random walk hypothesis, the extra data used in the first run contains no extra information on the desired delay estimates, and can only degrade the plasma delay estimate.

Thus the actual smoother performance supports the random walk hypothesis.

As an additional test, I compared the optimal linear smoother using the thin screen model (Run AP-48C) with the optimal linear smoother using the static model (Run AP-48G). As can be seen in Appendix I, use of the thin screen model does not improve the postfit residuals. The error in the plasma estimate is probably dominating any benefits from the thin screen model.

Chapter VI

Conclusions

In this thesis I have tried to describe the processing of plasma delay corrections for the Viking General Relativity Experiment, as well as a statistical study of dual-frequency measurements of plasma delays and delay rates. In Chapter IV, I hypothesized that the plasma delay can be, for the purposes of Lander plasma corrections, adequately modeled by a random walk, and in Chapter V, I tested this hypothesis on actual Lander plasma corrections.

Much work remains to be done with the Viking data. I am currently engaged in processing Viking Lander and Orbiter data covering the period from JD 2443420 to JD 2443804, which is not as straight forward as it might seem. The extension of the data span exposes inadequacies in the model of the Lander motions used in PEP. Use of S-band Orbiter Doppler data is required to break degeneracies exposed by the new Lander data. Another four hundred days of Lander data, including a second superior conjunction, remains to be processed. Other data, such as lunar laser ranging data, should be included in the solutions. There is currently a problem, possibly a program "bug", in the interpretation of Lander Doppler data. It is intended to commit a major effort in the near future to this problem. Some thought must also be given to plasma corrections for the Lander S-band Doppler data.

The General Relativity experiment is most sensitive to plasma corrections near superior conjunction. It might be possible to improve Lander plasma delay corrections near superior conjunction by hand validation of the appropriate SX Doppler data.

Unfortunately, current tests of solar system gravitational phenomenon do not have the level of precision needed to discriminate between various gravitational theories. It is generally acknowledged that an improvement in the precision of these tests by several orders of magnitude will be needed before the experimental tests have a direct impact upon the theorists. The chances of increasing the precision of the time delay test by the required amount are dim. At the very least round trip dual-frequency tracking of a Lander would be required to dramatically improve the accuracy of the plasma corrections. MU-2 machines would need to be placed at all three tracking station complexes. Considerable improvement would be required in the measurement of range calibrations (the RANCALs of Chapter III). With the current slowdown in the American space program, it is unlikely that such an experiment would be supported soon. Future high prcision tests of general relativity are likely to be conducted from Optical Interferometers in earth orbit (such as the MIT POINTS experiment).

Appendix I: Results of Parameter Solutions using Plasma Corrections*

Run ID	Root Mean Square Residual/ Errors	Number of Lander Delay Observations Used	Comments
AP-51	.489114	327	Standard parameter set plasma delay extrapolation
AP-37D	.350473	330	Corrected for lack of SX Bias
AP-42A	.347055	421	Uses old formal errors, uses points recovered by correcting range code errors
AP-42R	.346925	421	Identical to AP-42A except that the RELDEL parameter was included in the fit
AP-41C	.991057	330	Uses new formal error scheme
AP-41R	.97272	330	Identical to AP-41C except that the RELDEL parameter was included in the fit
AP-43C	1.00984	410	Identical to AP-42A except that the new formal errors are used and some lander points were deleted

*The Standard Parameter Set (see equation 5.2) is the default in the above, and consists of SPAN = 0.05 day

$C_1 = 1.0$

$C_2 = 1.0$

$C_3 = 0.1$

AP-48B	1.02357	410	ERROR in thin screen times corrected (see page 62) SPAN = 0.1 day
AP-48C	1.00984	410	Optimal linear smoother $C_3 = 10^6$, SPAN = 1 minute
AP-48E	5.30030	410	Average of extrapolated slopes with $C_3 = 10^6$, SPAN = 0.05 day
AP-48F	1.20653	410	Standard parameter set plasma delay interpolation
AP-48G	1.00984	410	Optimal linear smoother using static plasma model

Appendix II: The SXFILE Format

The SXFILE is the format chosen to store the SX range and Doppler data. Each SXFILE consists of an 80 byte header, used as an 80 character identifier, followed by an indefinite number of Range or Doppler SX data blocks in time order. Each data block is 96 bytes long and contains the epoch of observation, the observable itself, and various other information. Each SX range data block is followed by another 96 byte data block which contains the original S-band and X-band delay observables, the calibration values applied to the SX observable, the ranging code lengths used, and the output from the ranging correlators.

Information Storage Inside Each SXFILE Block

Name of Variable	Type	Purpose
TIME	R*8	Epoch of Observation TIME = Julian Date - 2440000
KIND	I*2	KIND {- 1 for range {- 3 for Doppler
NMOD	I*2	Number of modifications to this SX datum
SCNUM	I*2	S/C number
IQUAL	I*2	"Quality" of observation, relates to the nature of its calibrations
FREQ	R*8	Receiver synthesizer frequency - Hz
SX	R*8	S-X range observable S-3/11X Doppler
RUNID	R*8	
GENDTE	R*8	Used as 8 character run identifiers
MODDTE	R*8	
CLOCT	R*8	Range - Maximum Code Length Doppler - COUNT TIME
NCOMP	I*4	Range - number of ranging components Doppler - not used
IEE	I*4	Receiving station number
DSNAME	I*8	8 character receiving station name
NDOPTP	I*2	Doppler ground mode = 0 for range = 1 for one way Doppler = 2 for two way " = 3 for three way " = 4 for three way coherent "

14 trailing zero bytes

If data is range (KIND=1), a second record follows

Name of Variable	Type	Purpose
RANGE(2)	R*8	S range seconds X range
SHORTC(2)	R*8	S shortest codelength length X seconds
RANCAL(3)	R*8	S RANCAL values for this X observation S-X
IVOLTS(2)	I*4	In phase highest frequency Quadrature code phase - S-band
IVOLTX(2)	I*4	In phase highest frequency Quadrature code phase - X-band

24 trailing zero bytes

Appendix III: The Observation Library Tape and the Plasma Correction

OBServation LIBrary (OBSLIB) tapes are used to store delay, Doppler, and other measurements in a form suitable for use by PEP. Information on OBSLIB tapes is kept on 4 types of records. The Type I and Type II records occur only at the beginning of an OBSLIB tape. Measurements stored on the OBSLIB tape are grouped into series, which contain data with the same observed body, ground station, observable type, etc. One Type III record occurs at the beginning of each data series, and the measurements follow in time order, one for each Type IV record. Note that, although data within a series must be in time order, the series themselves can be in any order. Data series are numbered, and the series number is used for identification.

A variety of information is carried in each Type IV record. For the PREDICT runs in Chapter 5, this information includes the time tag of the observable, the observable itself, the residual (O-C), partials of the observable with respect to various parameters, and plasma corrections. The plasma and other propagation corrections are stored in the Type IV records on the CAL vectors. Three vectors and a scaler variable are used in storing the corrections:

NCAL The length of the vectors to be placed on the tape

CAL(I) Stores the actual correction

SCAL(I) Stores an error estimate of the actual correction

ICAL(I) Stores the rank of the correction; used in deciding which correction to use

The types of corrections and their positional assignments within the new vectors are as follows:

I	CORRECTION NAME	RANK	OBS. TYPE	
1	STATIC NEUTRAL ATMOSPHERE	2	TMDLY	C
2	STATIC NEUTRAL ATMOSPHERE	2	DOP	A I
				L N
3	ACTIVE TERRESTRIAL	2	TMDLY	C
4	NEUTRAL ATMOSPHERE	2	DOP	U P
				L E
5	PASSIVE TERRESTRIAL	3	TMDLY	A P
6	IONOSPHERE	3	DOP	T
				E
7	ACTIVE TERRESTRIAL	3	TMDLY	D
8	IONOSPHERE	3	DOP	
9	SOLAR PLASMA	1	TMDLY	
10	CALCULATED IN MEDIA	1	DOP	
11	STATIC SX FROM RNGNS	20	TMDLY	
12	CALIBRATIONS FROM DOPNS	20	DOP	
13	EXTRAPOLATED (in time)	17	TMDLY	
14	PLASMA CORRECTIONS (SX)	17	DOP	
15	RANGE CAL. VIA INTEGRATED S-X DOPPLER	18	TMDLY	
16	Not used			
17	RANCAL RANGE CALIBRATIONS	5	TMDLY	
19	EXTRATERRESTRIAL ATMOSPHERE	2	TMDLY	
21	SX CORRECTIONS FROM UPOLT	30	TMDLY	

The total propagation correction is a sum over appropriate elements in the CAL vector. This total correction is stored in a variable named SUMCOR.

The plasma correction, for the work reported on in this thesis, is provided by the UPOLT program. In general, the

OBSLIB tape input to UPOLT will have a plasma calibration already on it, generally in either CAL(15) or CAL(21). In that case, the old plasma correction must be replaced by the new plasma correction, the residual and theoretical observable must be changed, and NCAL also may need to be changed to reflect the increased size of the CAL vector.

If $SXCOR_{new}$ is the new plasma correction, calculated in UPOLT (see Equation 4.24), and $SXCOR_{old}$ is the old plasma correction, from the CAL vector, then the update equations are

$$Computed_{new} = Computed_{old} + SXCOR_{new} - SXCOR_{old}$$

$$Residual_{new} = Residual_{old} - SXCOR_{new} + SXCOR_{old}$$

$$SUMCOR_{new} = SUMCOR_{old} + SXCOR_{new} - SXCOR_{old}$$

The new plasma correction is placed in the 21th slot of the CAL vector, which is stored on the new OBSLIB tape.

Appendix IV: Conversion between Julian Date and Civil Date

Julian Date	Civil Date	Comments
2442779	1 January 1976	
2442931	1 June 1976	
2442980	20 July 1976	VL1 Lands on Mars
2443025	3 September 1976	VL2 Lands on Mars
2443108	25 November 1976	Superior Conjunction
2443145	1 January 1977	
2443296	1 June 1977	
2443420	3 September 1977	End of Data Span used in this Thesis
2443510	1 January 1978	
2443667	1 June 1978	
2443875	1 January 1979	
2443895	21 January 1979	Superior Conjunction
2444026	1 June 1979	

References

1. Shapiro, I. I., R. D. Reasenberg, P. E. MacNeil, R. B. Goldstein, J. P. Brenkle, D. L. Cain, T. Komarek, A. I. Sygielbaum, W. F. Cuddihy, and W. H. Michael, Jr., "The Viking Relativity Experiment," Journal of Geophysical Research, Vol. 82, # 28, pp. 4329-4334, 1977.

2. Goldstein, R. M., "Ranging with Sequential Components," JPL Space programs Summary 37-52, Vol. II, pp. 46-49, 1968.

3. Martin, W. L., "A Binary Coded Sequential Acquisition Ranging System," JPL Space programs Summary 37-57, Vol. II, pp. 72-81, 1969.

4. Martin, L. L., "system Performance of the Dual Channel MU-II Sequential Ranging," JPL Viking RO13, 1976.

5. Komarek, T., and T. Otoshi, "Terminology of Ranging Measurements and DSS Calibrations," JPL Deep Space Network Progress Report 42-36, pp. 35-40, 1975.

6. Jackson, J. D., Classical Electrodynamics, Chapter 7, John Wiley and Sons, 1975.

7. Harwit, M., Astrophysical Concepts, Chapter 6, John Wiley and Sons, 1973.

8. Jokipii, J. R., "Turbulence and Scintillations in the Interplanetary Plasma," Annual Review of Astronomy and Astrophysics Volume 11, pp 1-28, 1973.

9. Pizzo, V., "A Three-Dimensional Model of Corolating Streams in the Solar Wind," Journal of Geophysical Research, Vol. 83, pp. 5563-5572, 1978.

10. van de Hulst, H. C., "The Electron Density of the Solar Corona," Bull. Astron. Soc. Nether. Vol. XI, # 410, pp. 135-150, 1950.

11. Tyler, G. L., J. P. Brenkle, T. A. Komarek, and A. I. Zygielbaum, "The Viking Solar Corona Experiment," J. Geophys. Res., Vol. 82, # 28, 1977.

12. Kraus, J. D., Radio Astronomy, Chapter 5, McGraw-Hill, 1966.

13. Nash, R. A. and S. K. Jordan, "Statistical Geodesy - An Engineering Perspective," Proc. IEEE, Vol. 66, # 5, pp. 532-550, 1978.

14. Box, G. E. P., and G. M. Jenleins, Time Series Analysis-Forecasting and Control, revised ed, Holden Day, 1976.

15. Gelb, A., editor, Applied Optimal Estimation, MIT Press, 1974.

16. Eubanks, T. M., and R. Goldstein, Memo on Plasma Corrections, 2 February 1977.

17. Reasenberg, R. D., and R. W. King, The Rotation of Mars, J. Geophys. Res., Vol. 84, # B11, Oct. 10, 1979.

18. Ash, M. E., "Determination of Earth satellite Orbits," Lincoln laboratory Technical Note 1972-5, 1972.

19. Jazwinski, A. H., Stochastic Process and Filtering Theory, Academic Press, 1970.

20. Tyler, G. L., J. P. Brenkle, T. A. Komarek, and A. I. Zygielbaum, The Viking Solar Corona Experiment, J. Geophys. Res., Vol. 82, 4335-4340, 1977.

21. Shapiro, I. I., Fourth Test of General Relativity, Phys. Rev. Lett., 13, 789-791, 1964.

22. Martin, W. L., and J. W. Layland, Binary Sequential Ranging with Sine Waves, JPL Deep Space Network Progress Report 42-31, pp. 30-40.

23. Reasenberg, R. D., I. I. Shapiro, P. E. MacNeil, R. B. Goldstein, J. C. Breidenthal, J. P. Brenkle, D. L. Cain, T. M. Kaufman, T. A. Komarek, and A. I. Zygielbaum, Viking Relativity Experiment: Verification of Signal Retardation by Solar Gravity, Ap. J., Vol 234: L219-L221, Dec. 15, 1979.

24. Dunsmair, W., P. M. Robinson, Asymtotic Theory for Time Series Containing Missing and Amplitude Modulated Data, 1979, to be published.

Figure 1) The Observation Geometry

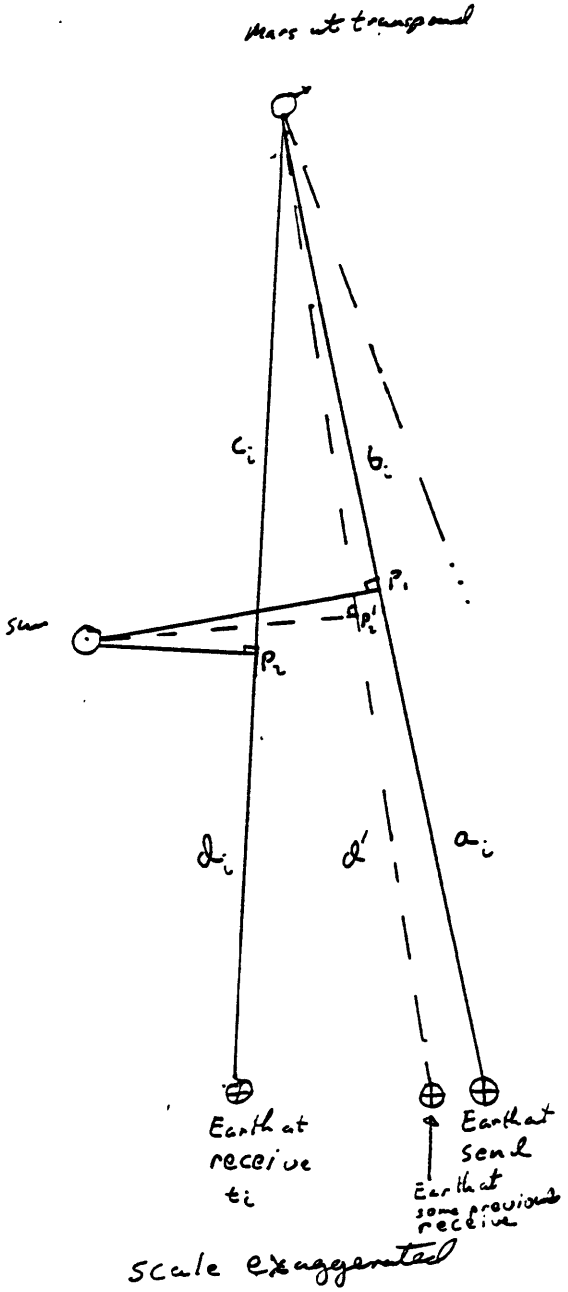

Figure 2) Simplified Ranging System Block Diagram

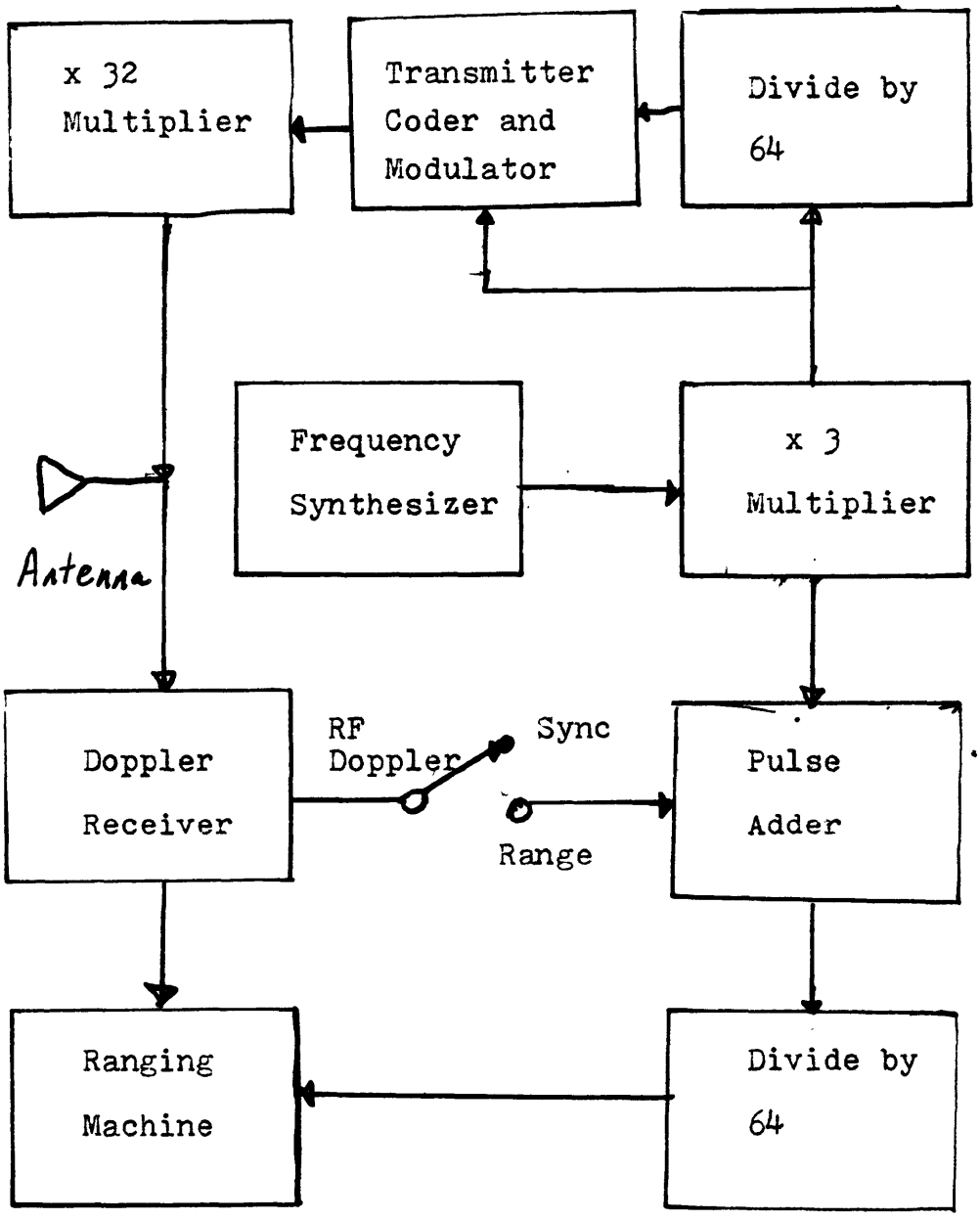

Figure 3) Idealized Ranging Receiver
Correlator Output

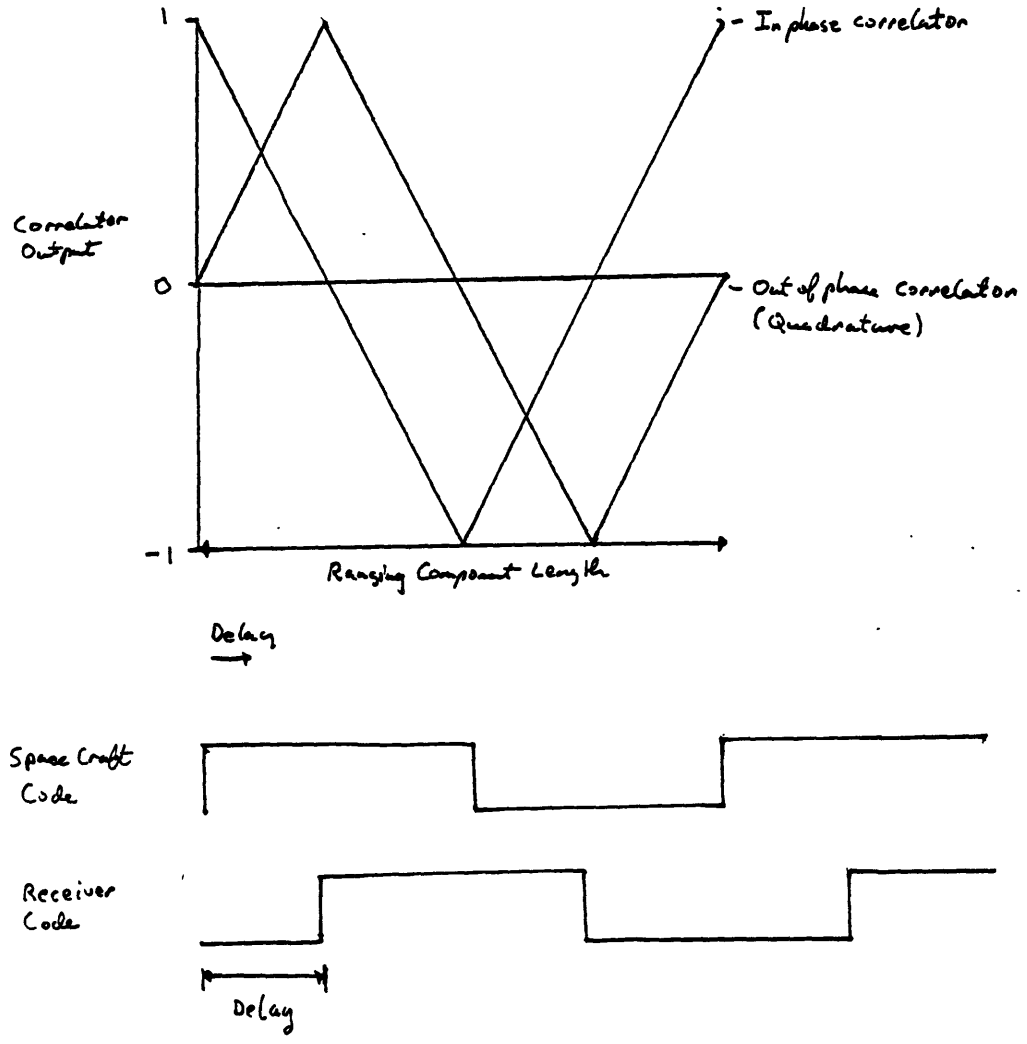

Figure 4, ATDF Data Flow Stream

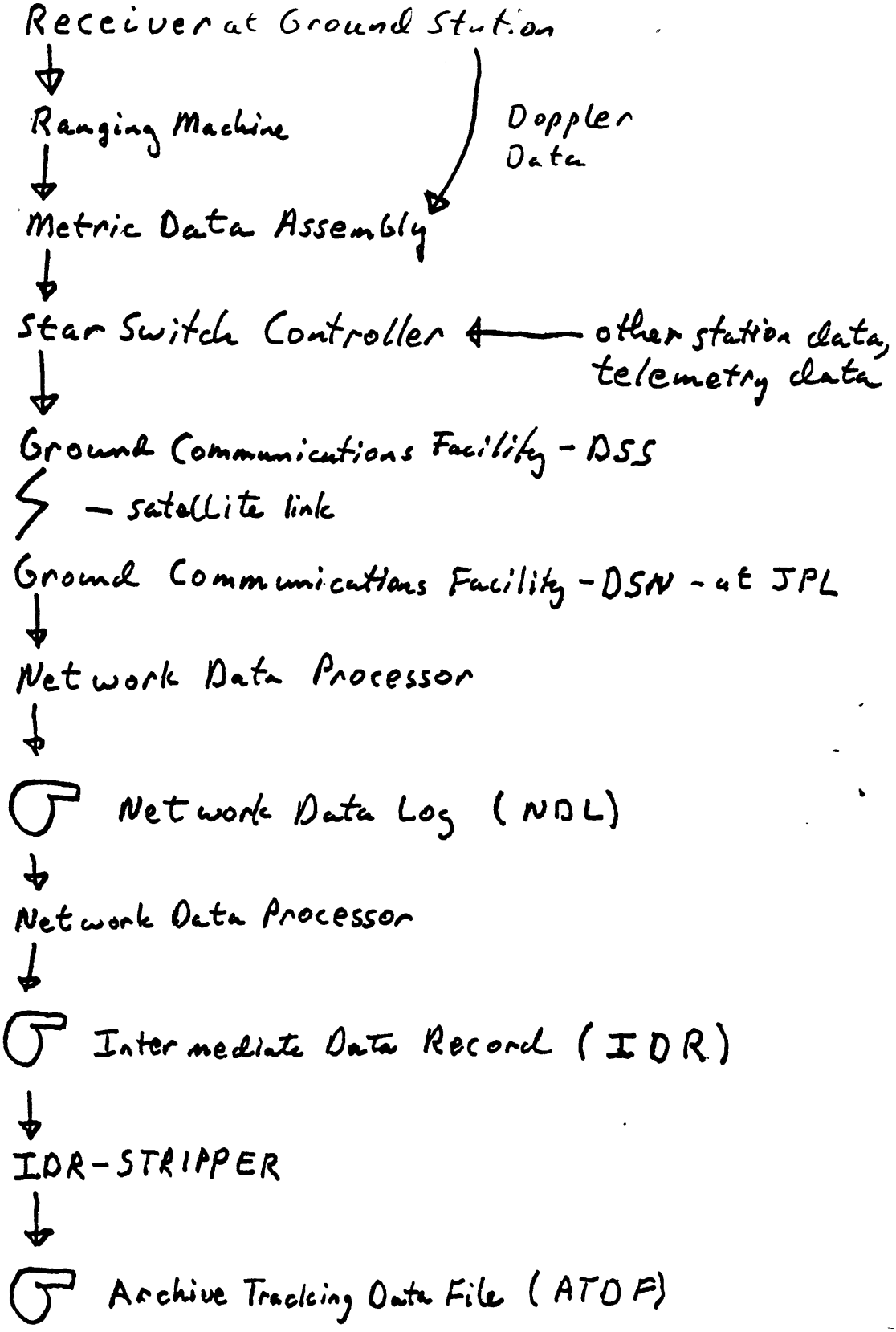

Figure 5) V11 Rancals

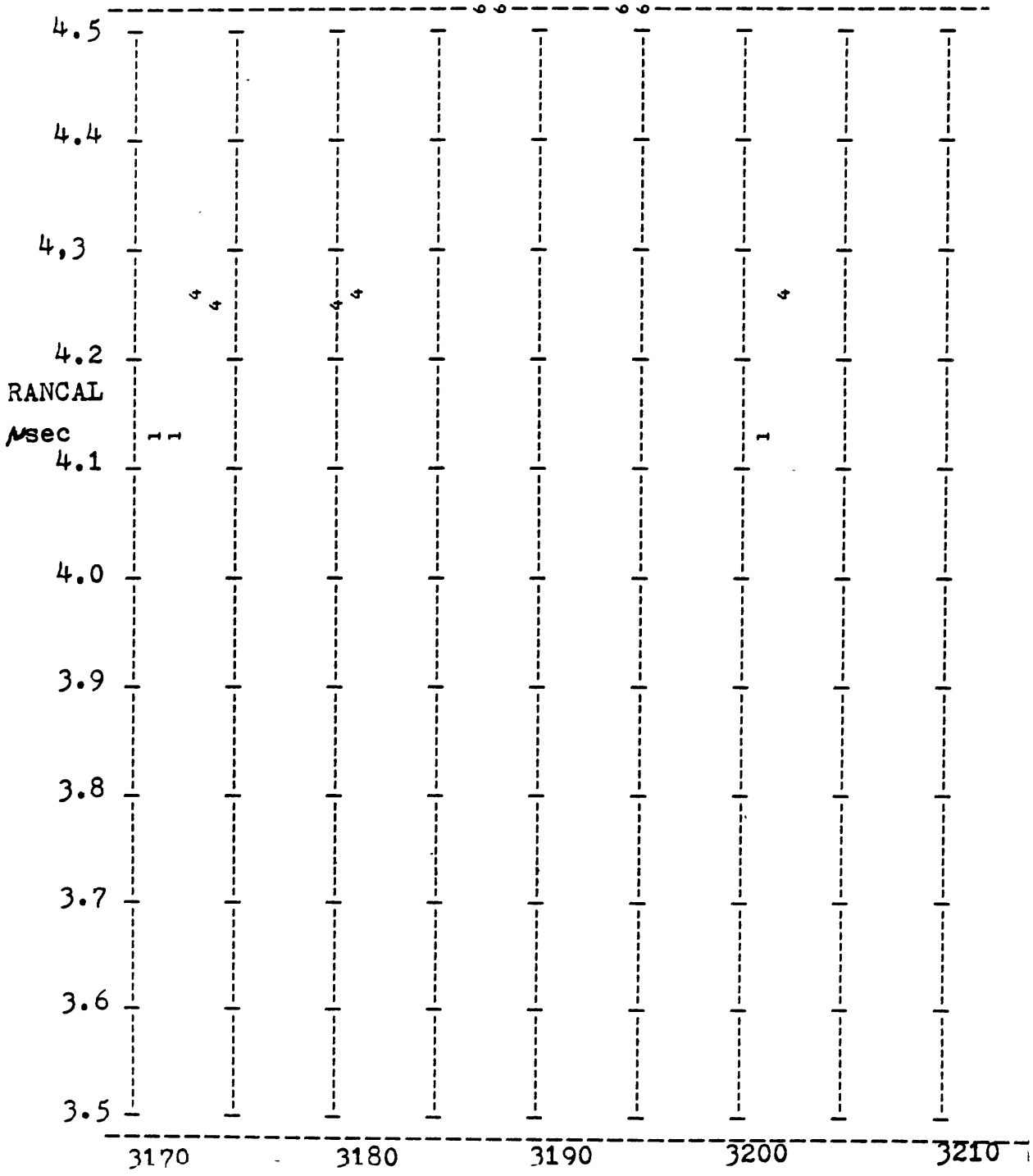

Figure 6) The Geometry of the DSS Correction

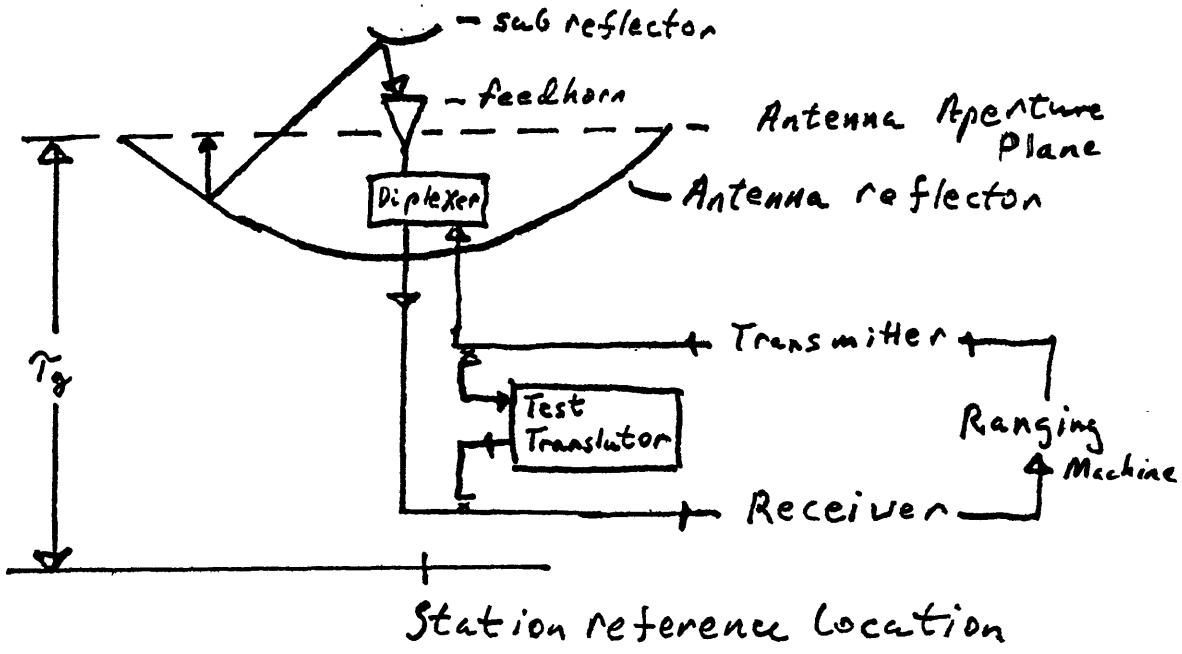

Figure 7) SX Delay Data Processing at M.I.T.

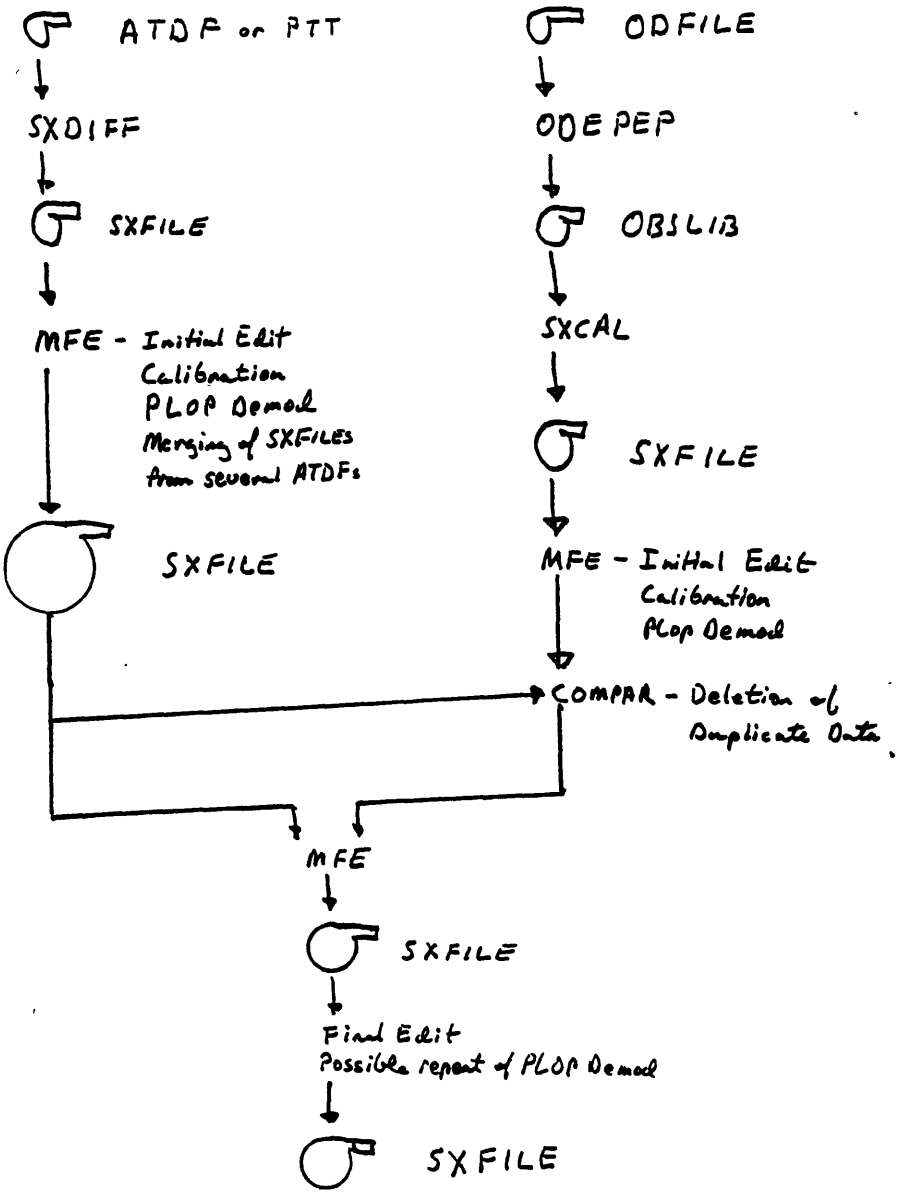

Figure 8) Plot of bad data group

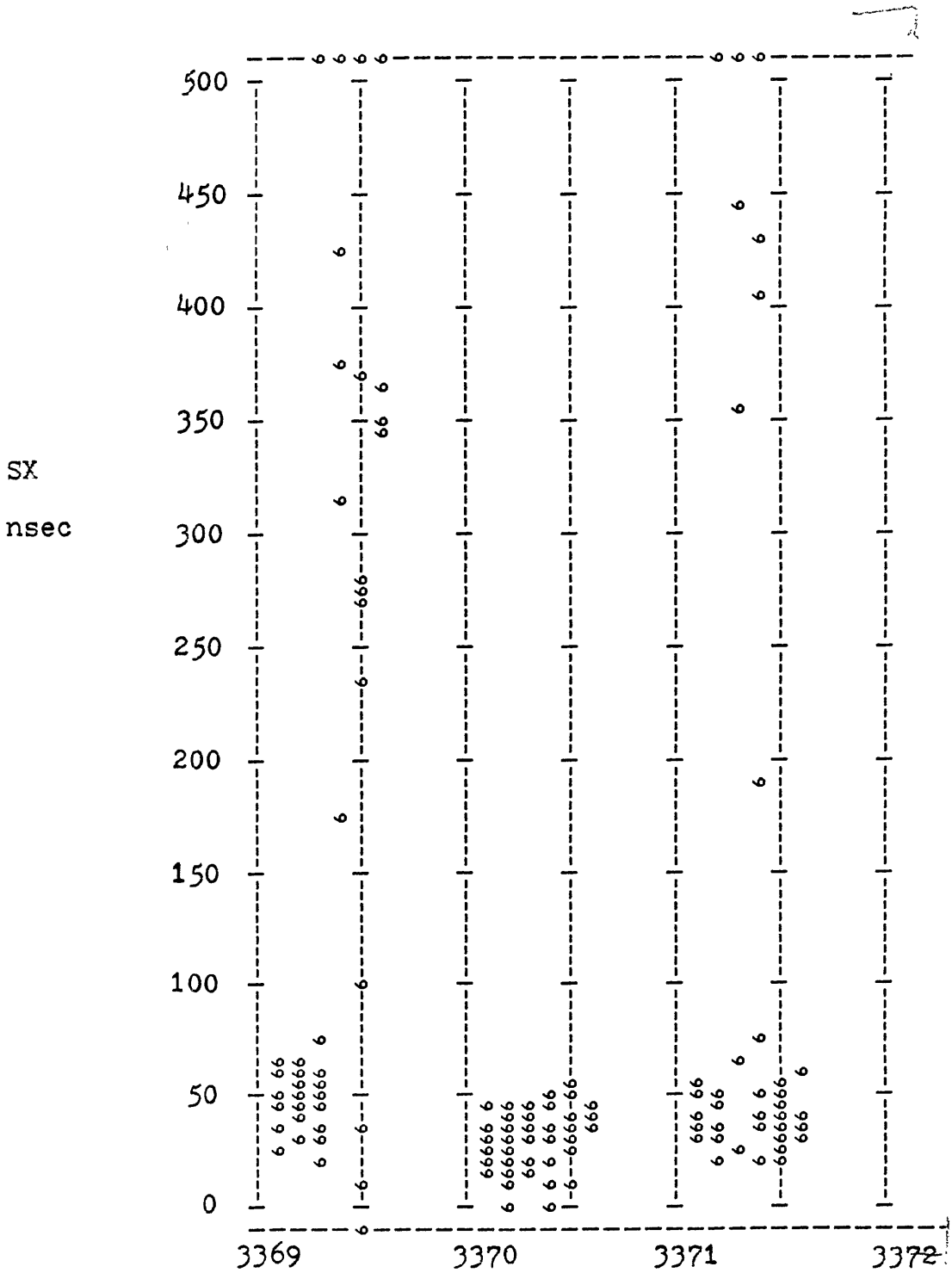

Figure 9) Plot of isolated bad datum

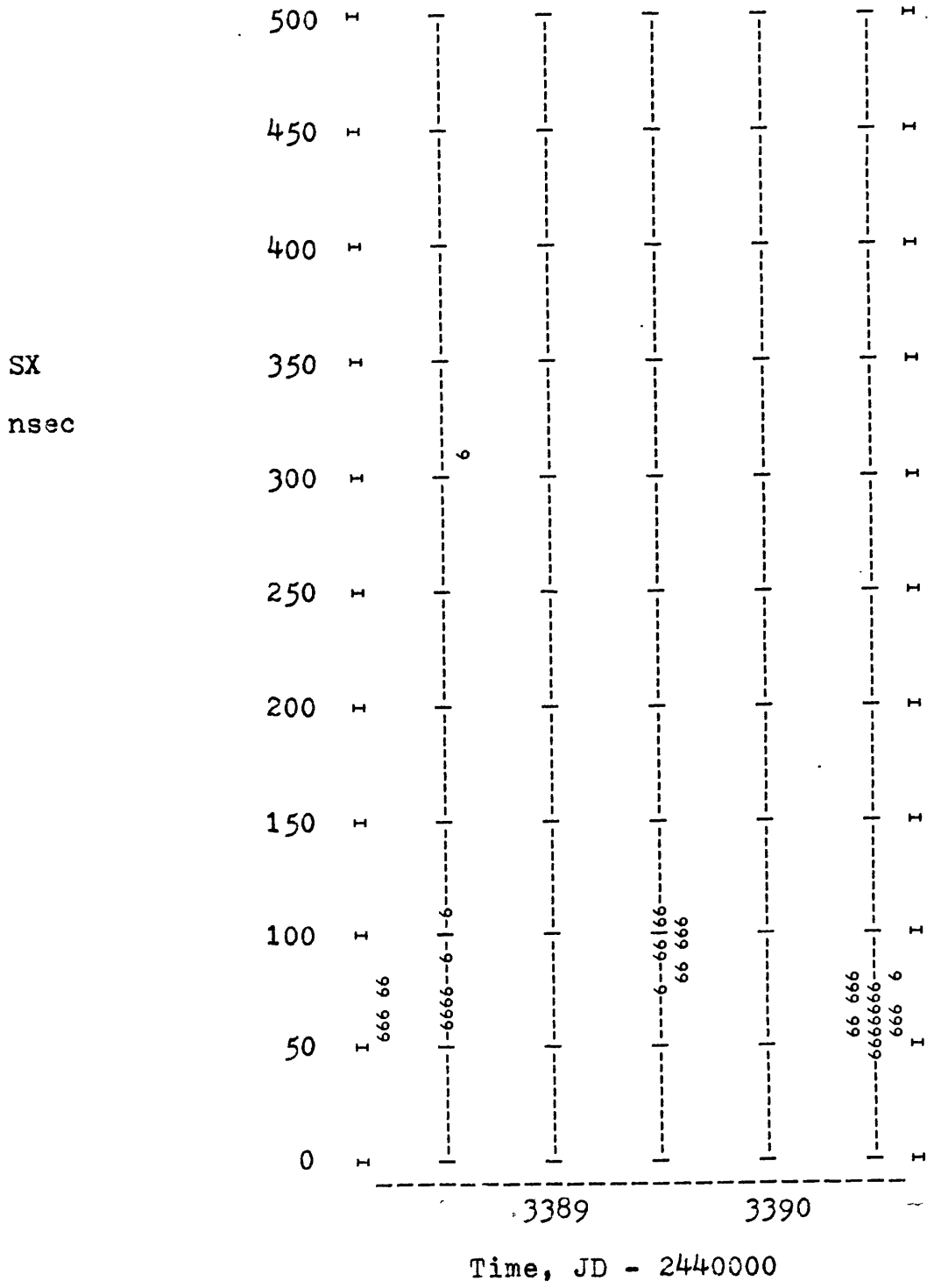

Figure 10) Overlapping Integrated SX Doppler

Before Deletions

1 - VO-1

· - VO-2

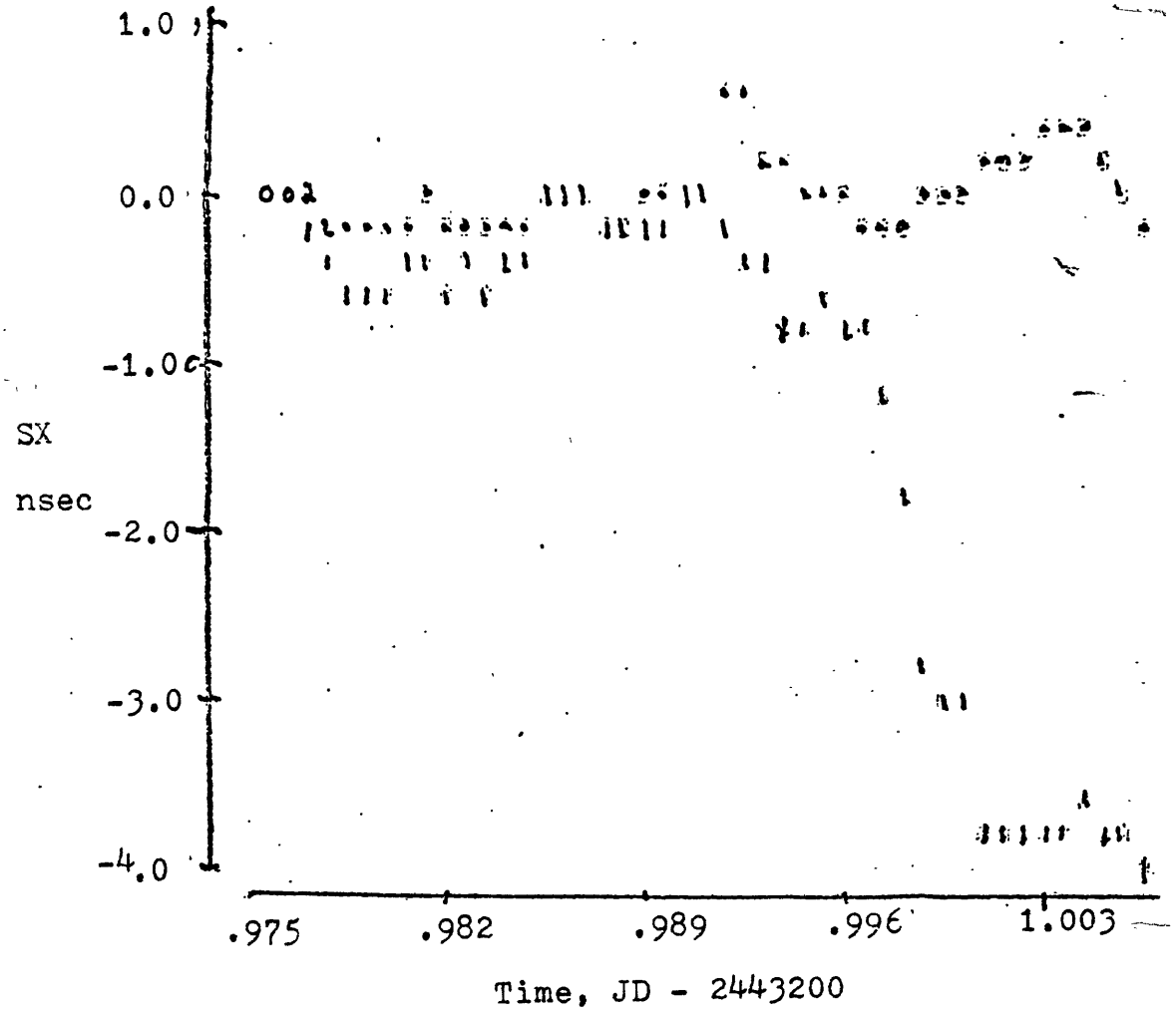

Figure 11) Overlapping Integrated SX Doppler

After Deletions

1 - V0-1

2 - V0-2

0 - Overlap

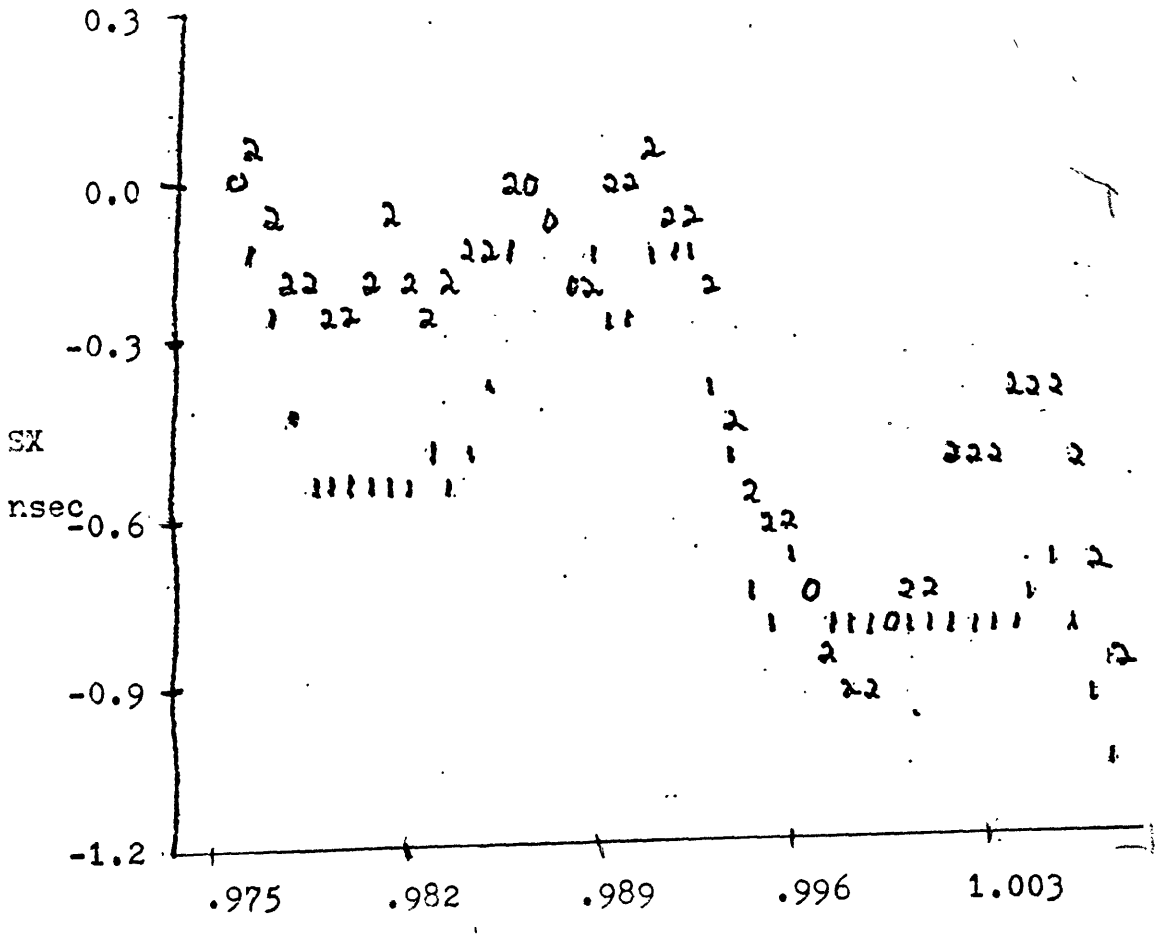

Figure 12 SX range vs. time near Superior Conjunction

Superior Conjunction ≡ JD 2443108 or Nov. 25, 1976
1 - DSN 14
4 - DSN 43
6 - DSN 63

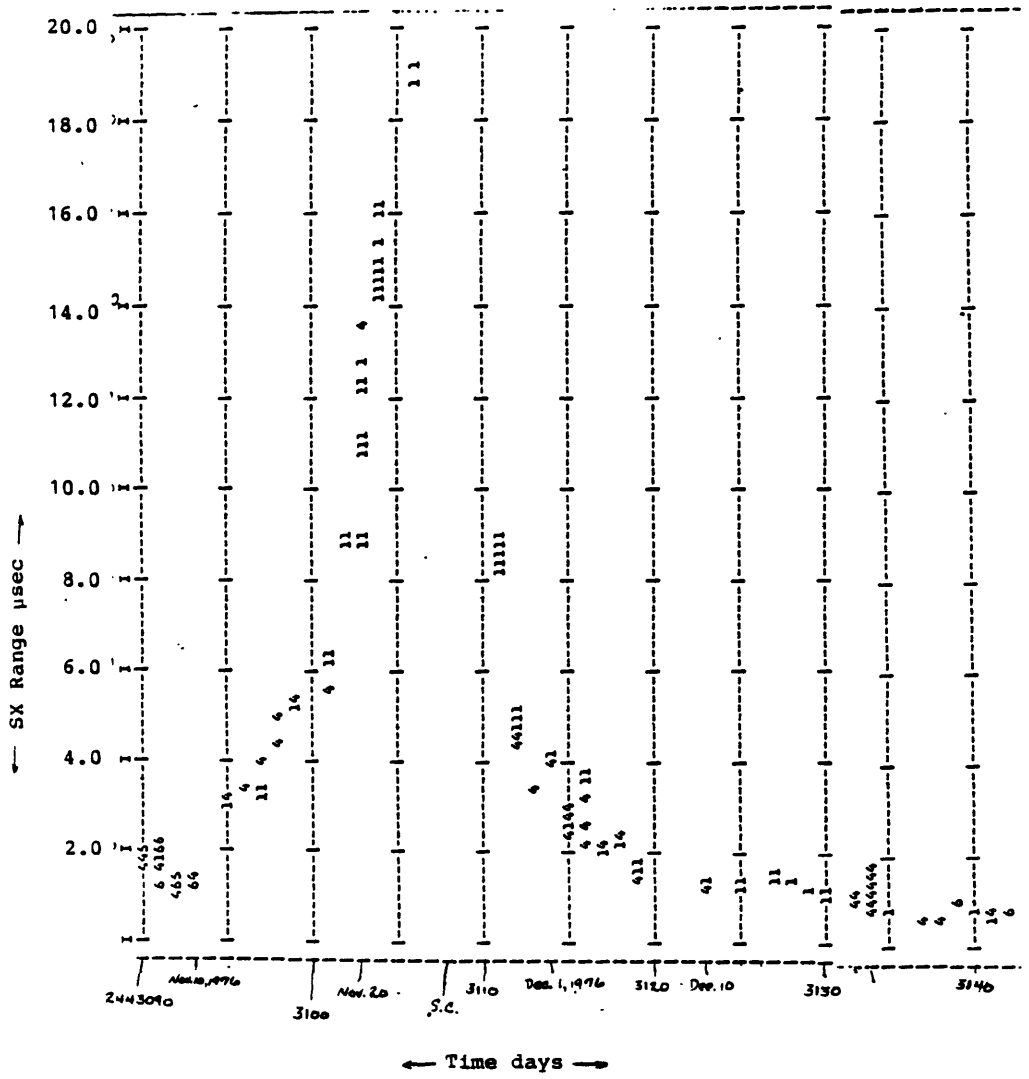

Figure 13) SX Range from VO1 DSN 43 on JD 2443110 to JD 2443111
Nov. 27-28, 1976, 2 days after Superior Conjunction

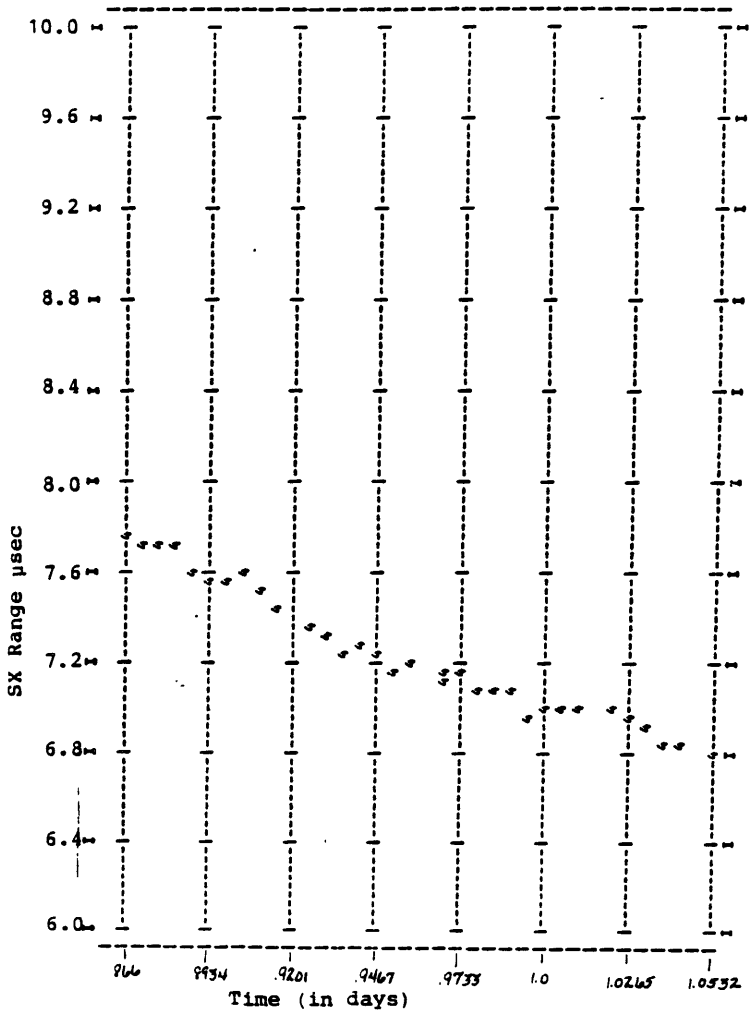

Data taken at 7 min 30 sec intervals
Time = Julian date - 2443110.0

Figure 14) SX' = SX range/H(ℓ) for VO1 DSN 43 (see Eq. 4.9)
on JD 2443110 to 2443111
Nov. 27-28, 1976

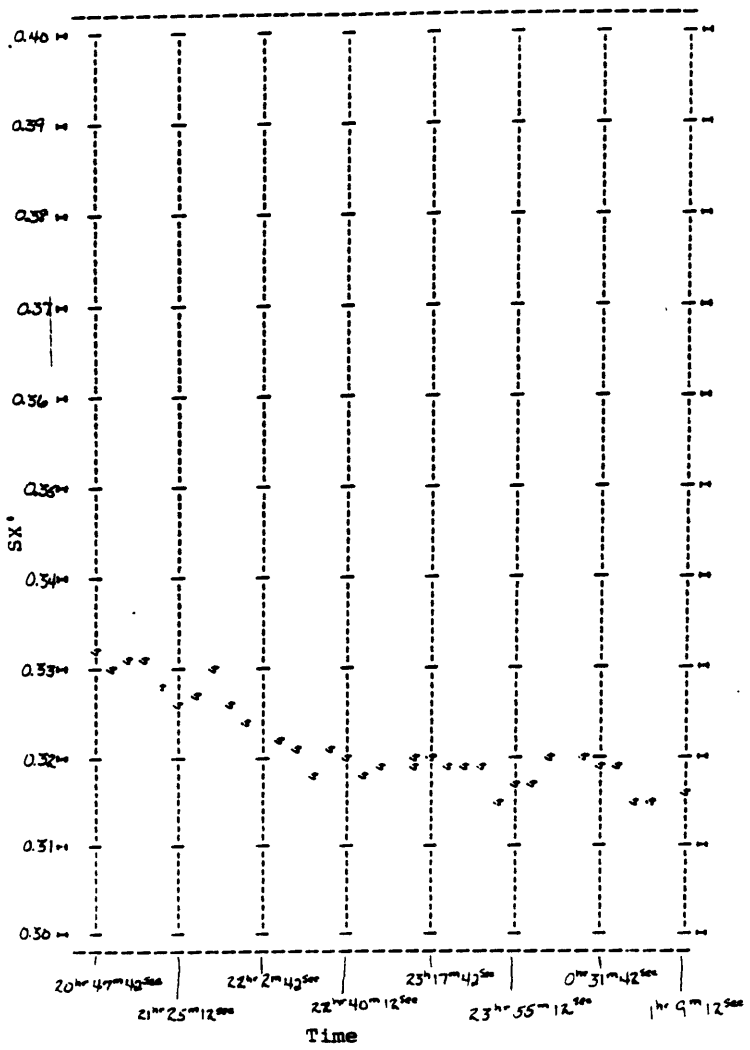

Time of day on Nov. 27, 28, 1976

Figure 15½ SX' = SX/H(ℓ) Autocorrelation

t_1 = 2443058

t_2 = 2443158

Δt = 0.1 day

Mean subtracted from SX' sequence
Straight line provided for reference only

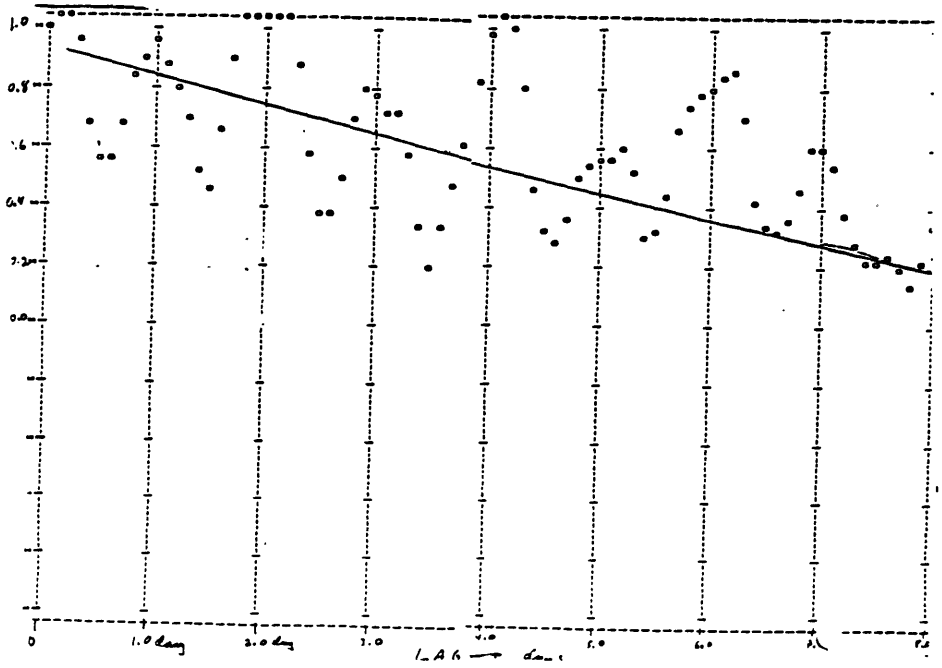

Lag ⟶ days

Figure 16a) Correlation of First Differences of SX' = SX/H(ℓ)

t_1 = JD 2443058

t_2 = JD 2443158

Δt = 0.1 day

(the mean was subtracted from the Differenced Sequence)

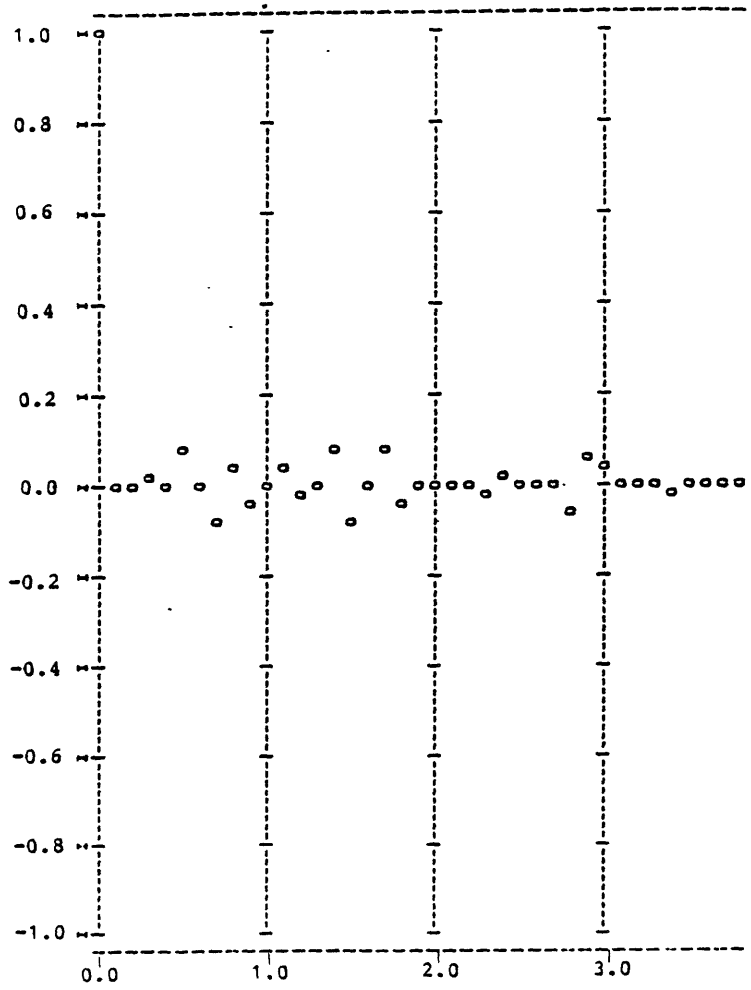

Note: This is over the same data used in Figure 15.

Figure 16b Correlation of First Difference of SX' = SX/H(ℓ)

t_1 = JD 2443350

t_2 = JD 2443400

Δt = 0.01 day

5107 Range Differences
The mean was not subtracted from this sequence

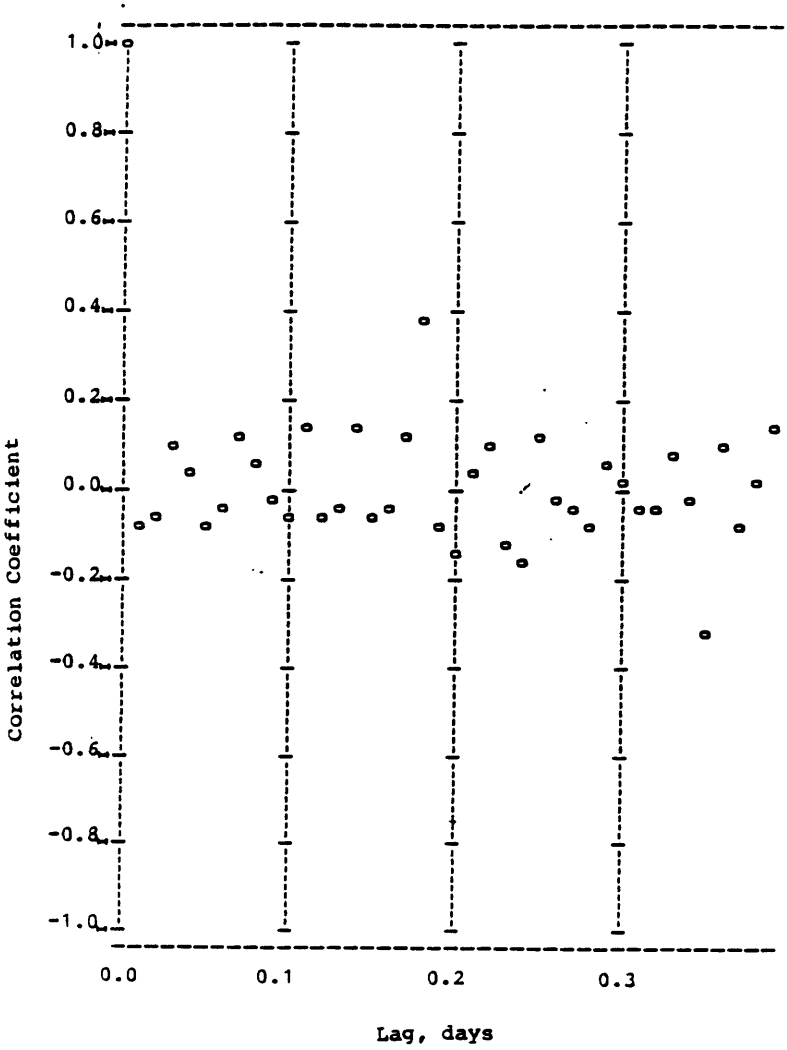

Figure 17) Plot of Integrated SX Doppler
Circled points are Delay

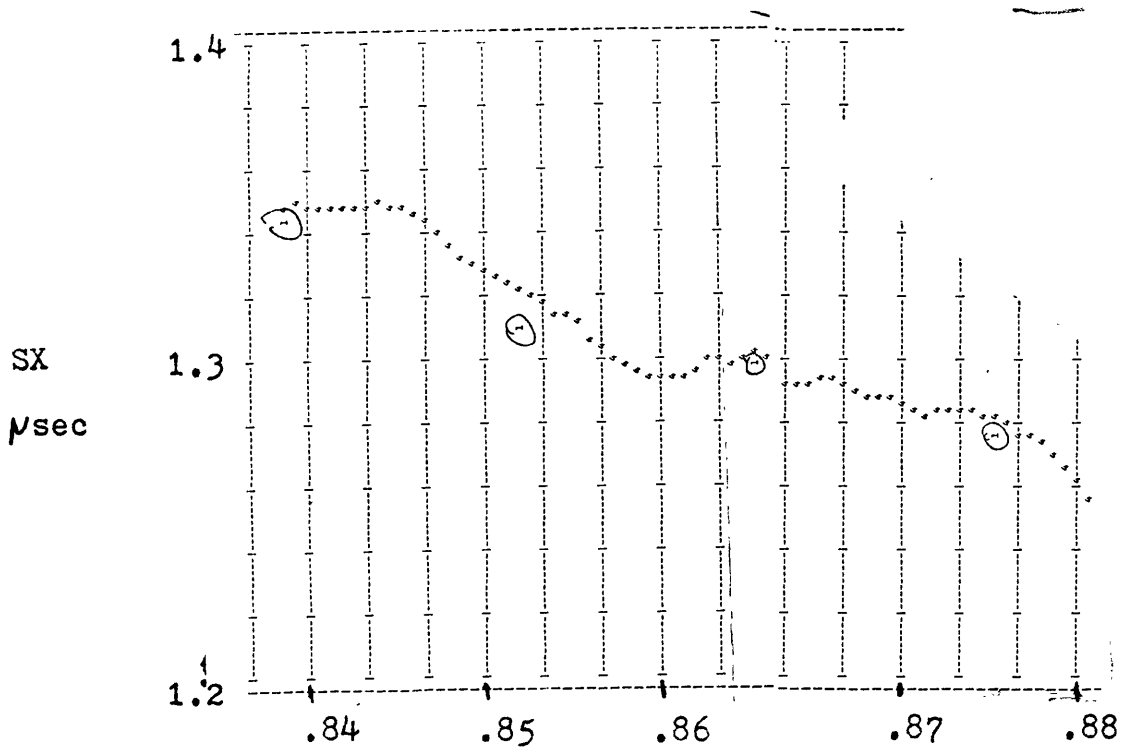

Figure 18a) Autocorrelation of SX Doppler

t_1 = JD 2443095.353

t_2 = JD 2443095.595

Δt = 1 minute

349 VO2 SX Doppler Observations
The mean was subtracted from this data sequence

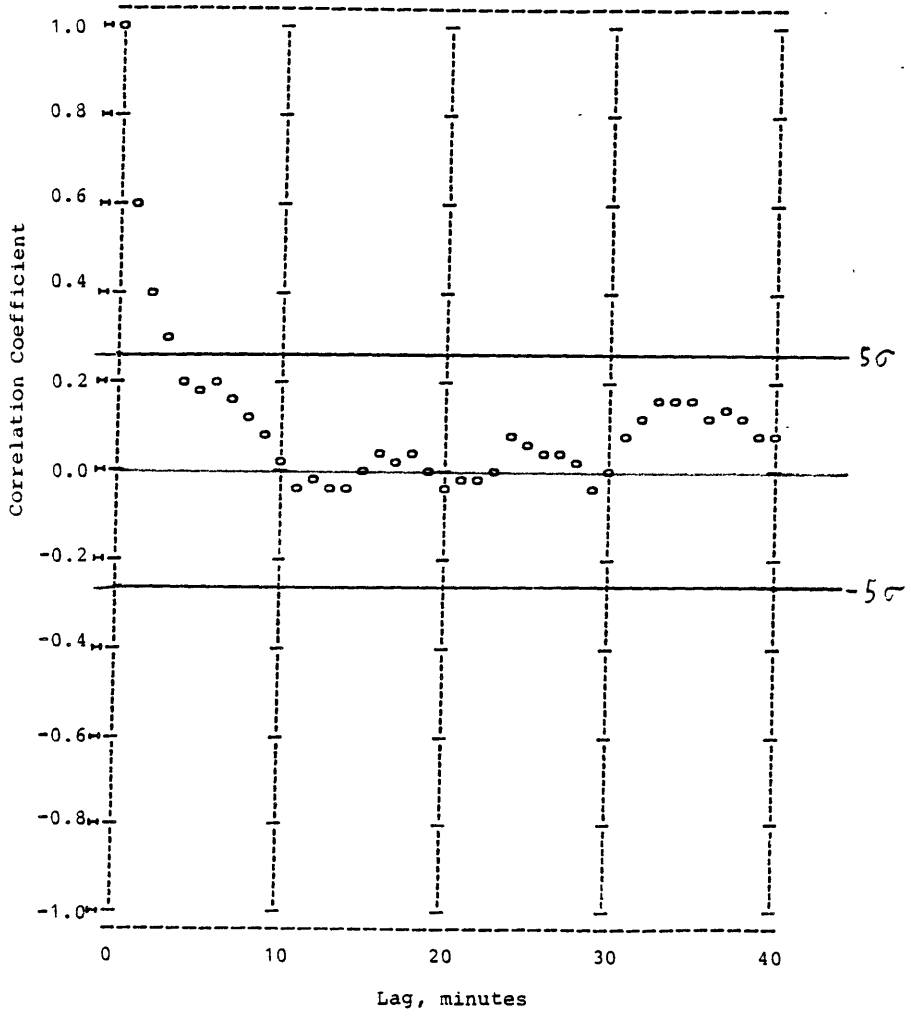

Figure 18b) Autocorrelation of SX Doppler Data

t_1 = JD 2443101.080

t_2 = JD 2443101.347

Δt = 1 minute

383 SX Doppler Observations - all VO2
The mean was subtracted from this data sequence

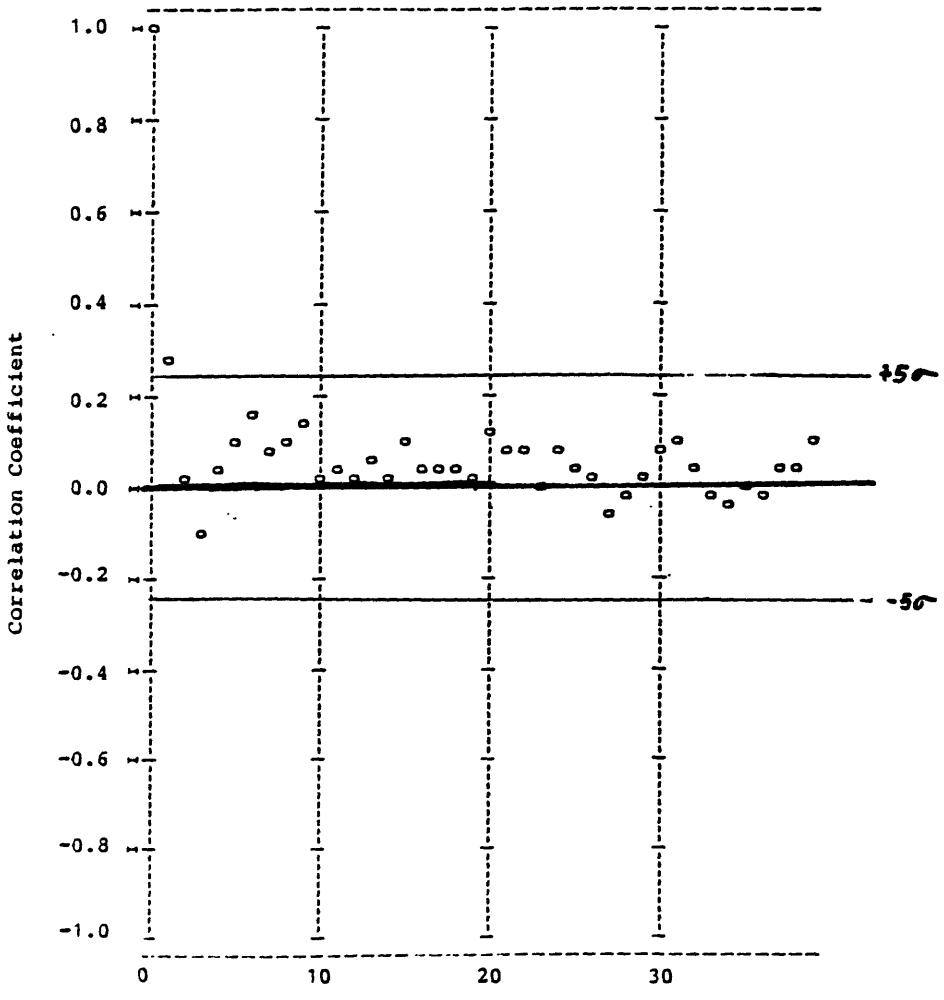

Figure 18 c) Autocorrelation of SX Doppler Data

t_1 = JD 2443117.685

t_2 = JD 2443117.800

Δt = 1 minute

166 Observations from VO-2

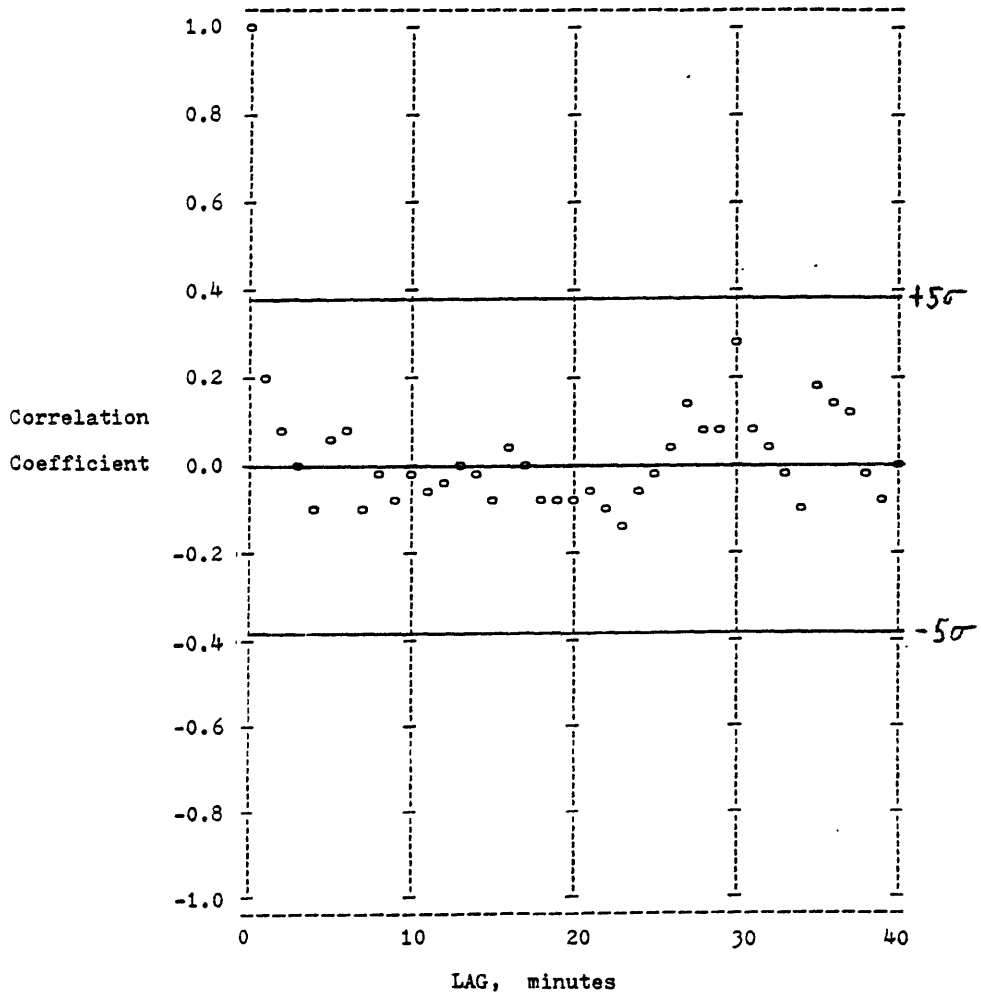

Figure 18 d) Autocorrelation of SX Doppler Data

t_1 = JD 2442124.839

t_2 = JD 2443124.9577

Δt = 1 minute

171 Observations from VO-1

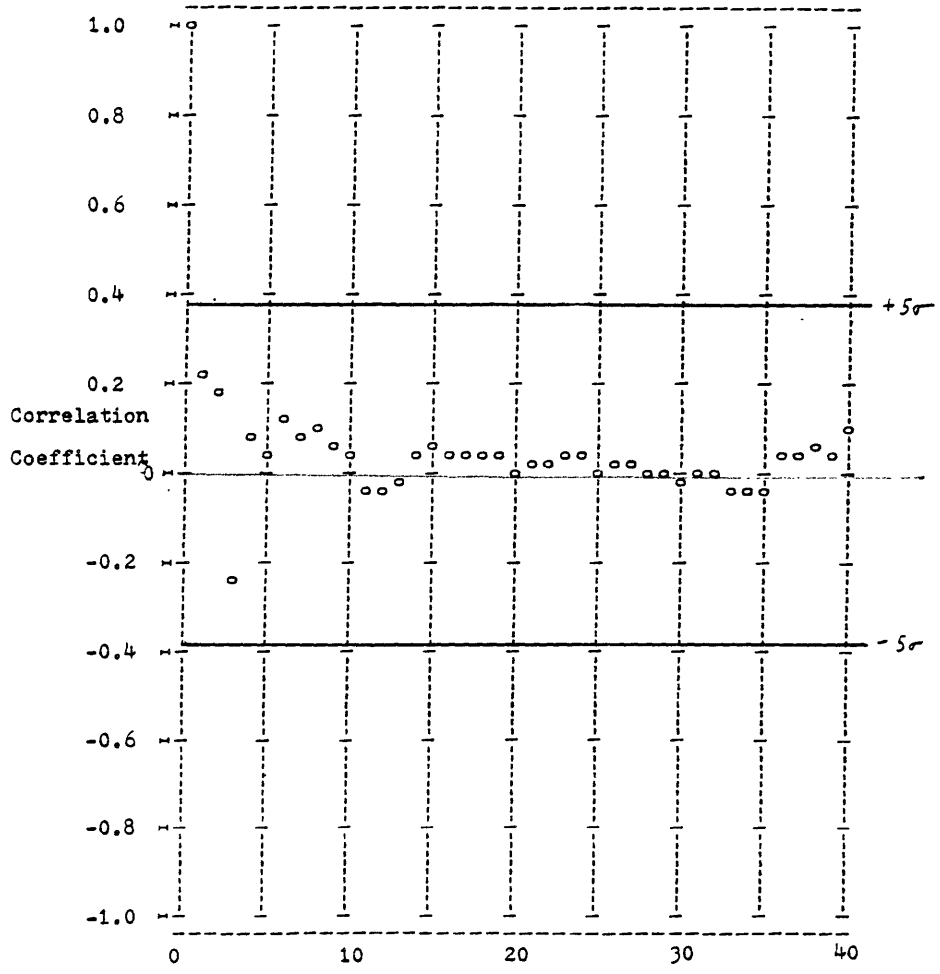

Figure 18 e) Autocorrelation of SX Doppler Data

t_1 = JD 2443160.8851

t_2 = JD 2443161.317

Δt = 1 minute

606 Observations from VO-1

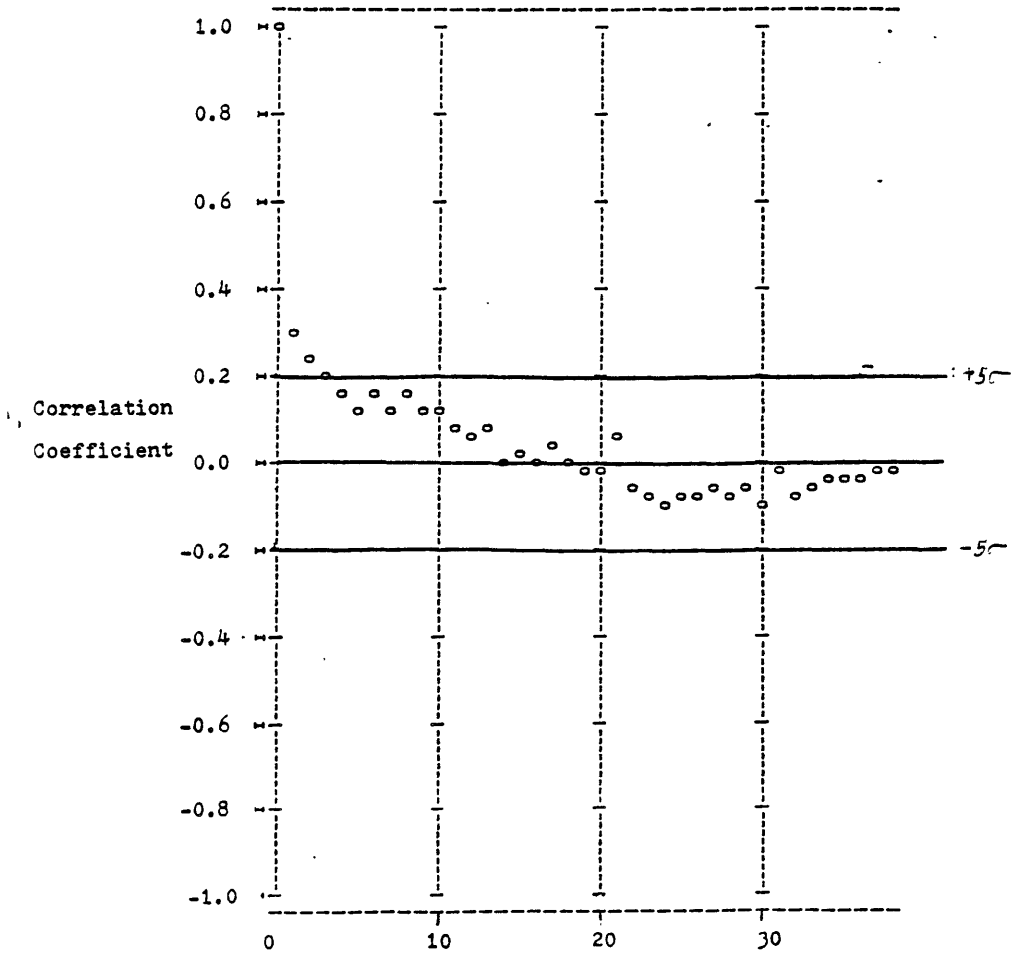

Figure 19a) Residual Plot from Run AP-48F
Standard Parameter Set Plasma Delay Interpolation

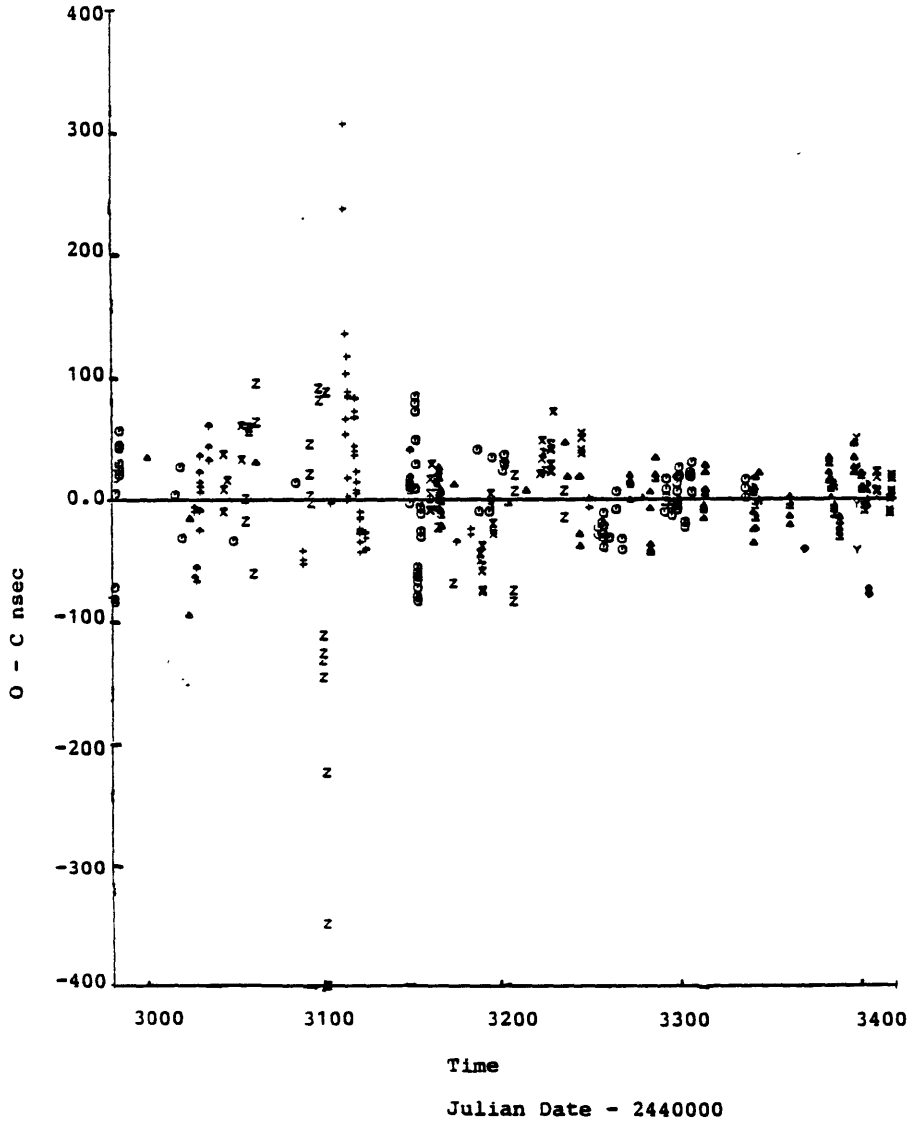

Figure 19b) Residual Plot from run AP-48C Optimal Linear Smoother with Thin Screen Plasma Model

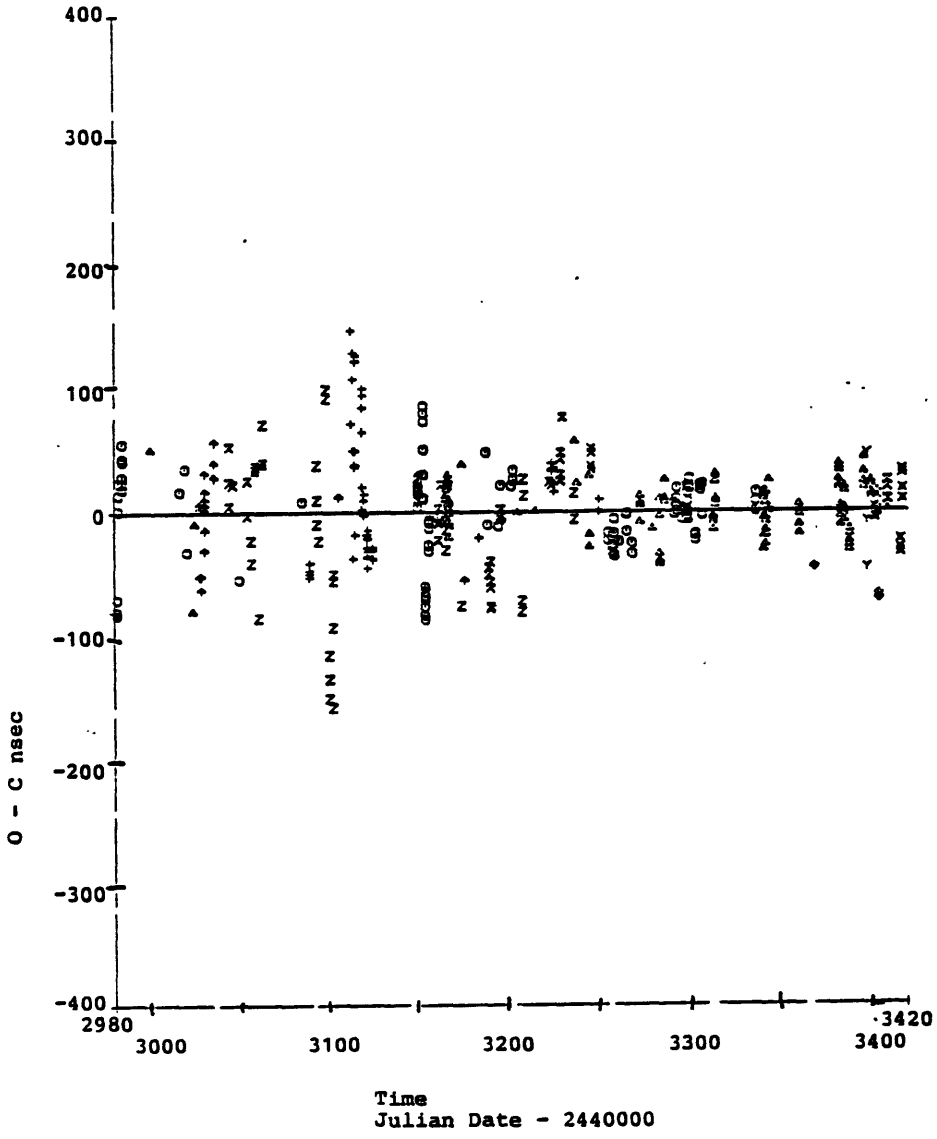

Figure 19c) Residual Plot from run AP-48E Plasma Correction in Average of Extrapolated Slopes

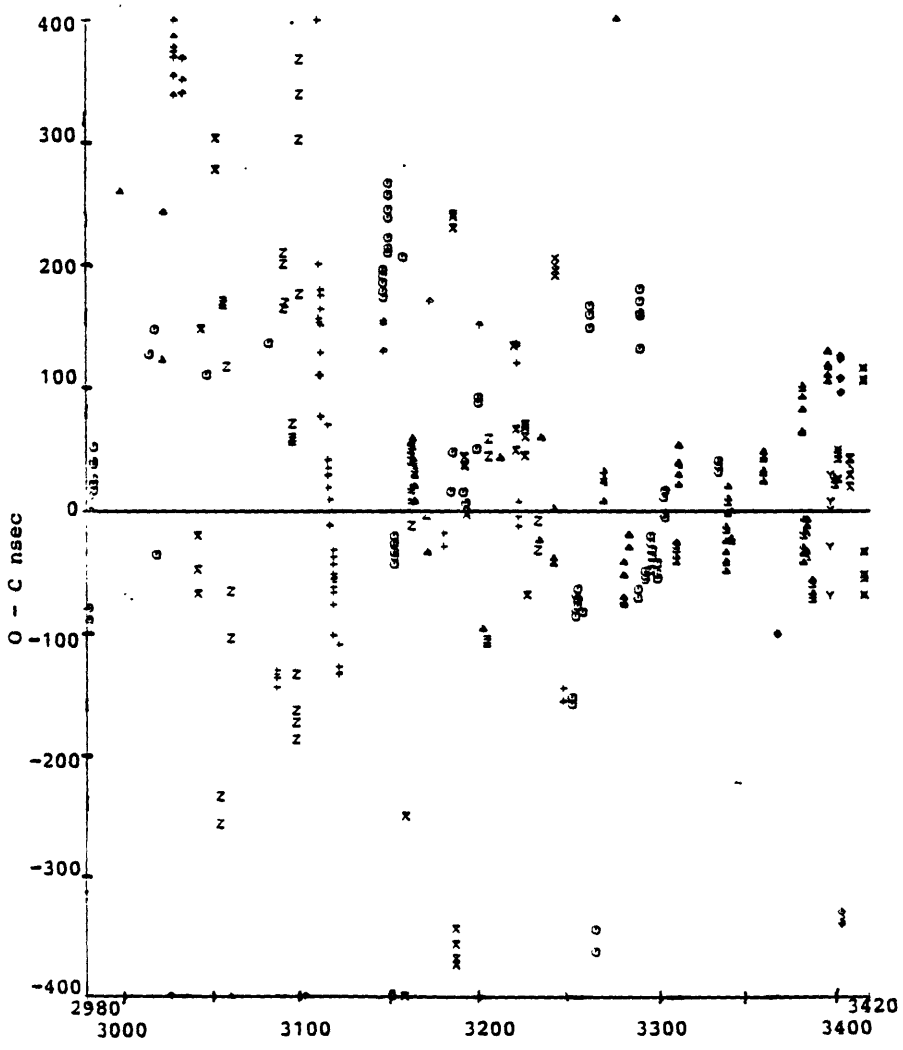

Figure 19d) Residual Plot from run AP-48G Optical Linear Smoother Using Static ($P_{up} = P_{down}$) plasma model.

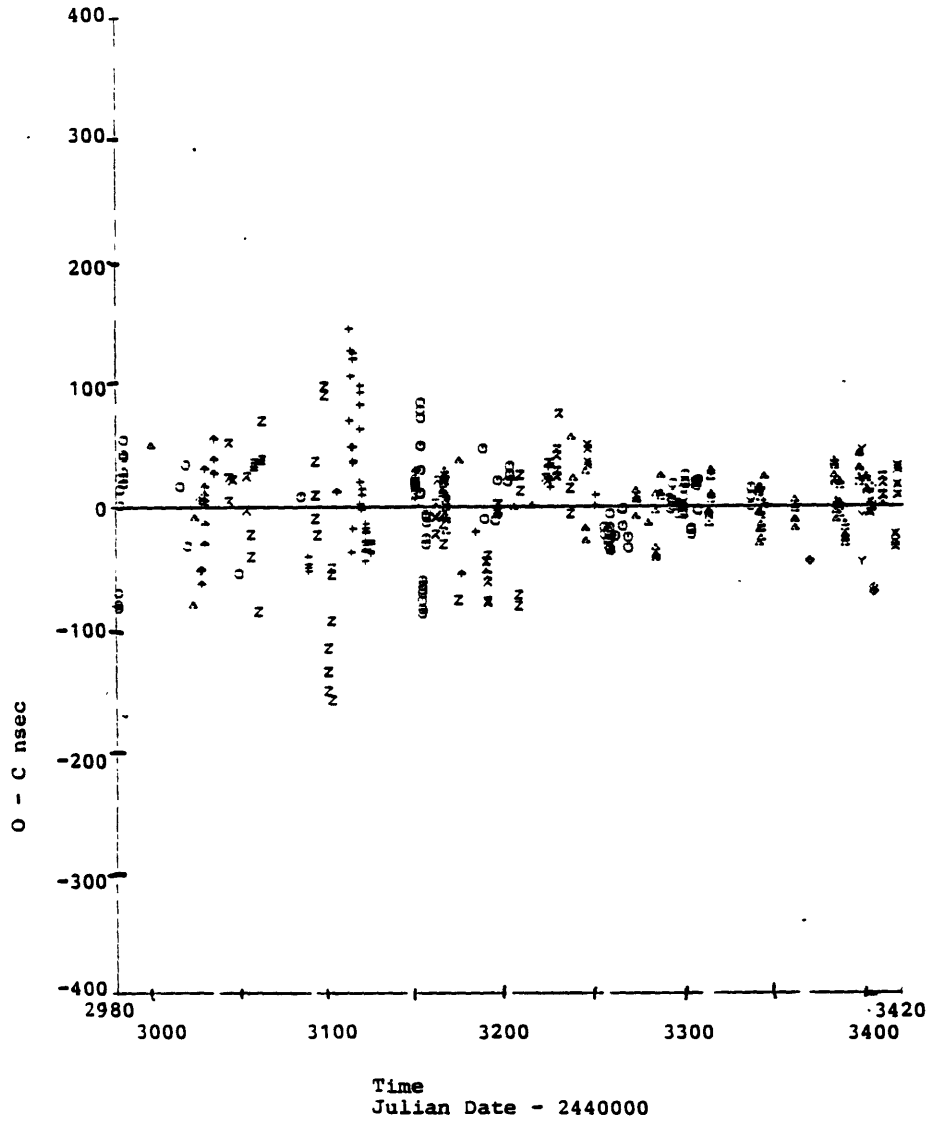

Figure 20 (a) HOG Output

Residual Scatter versus δT_{SC}

410 Lander Range Residuals
Bin Width = 10 days
Date of Superior Conjunction: JD 2443108
or November 25, 1976

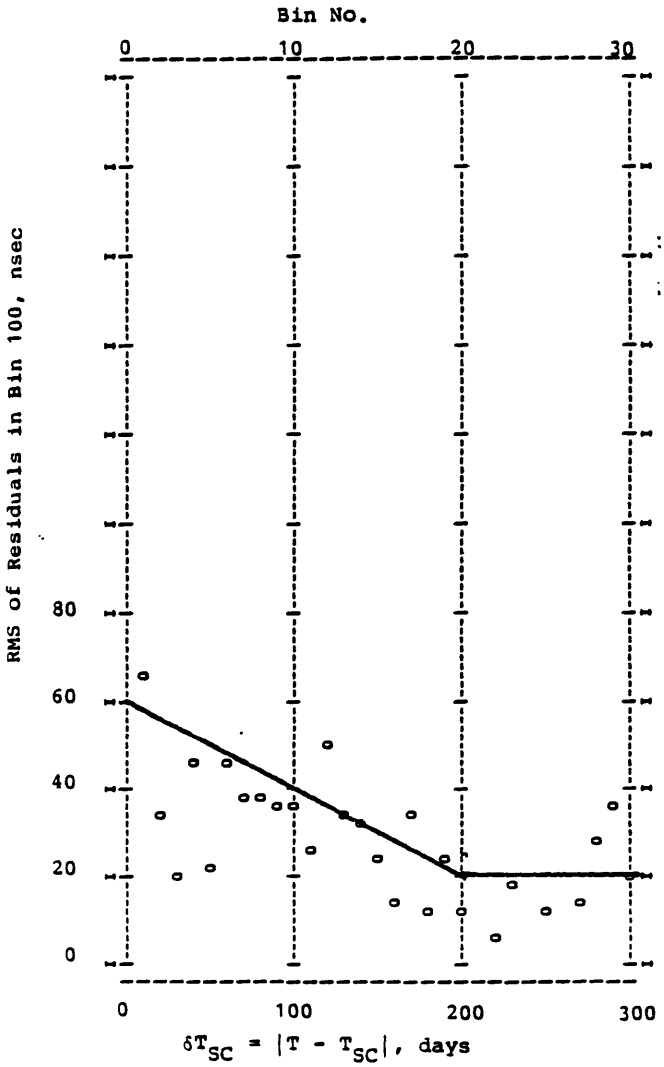

Figure 20 b) Histogram of Number of Lander Observations versus Time to Superior Conjunction for Run AP-48C. Bin Width = 10 Days

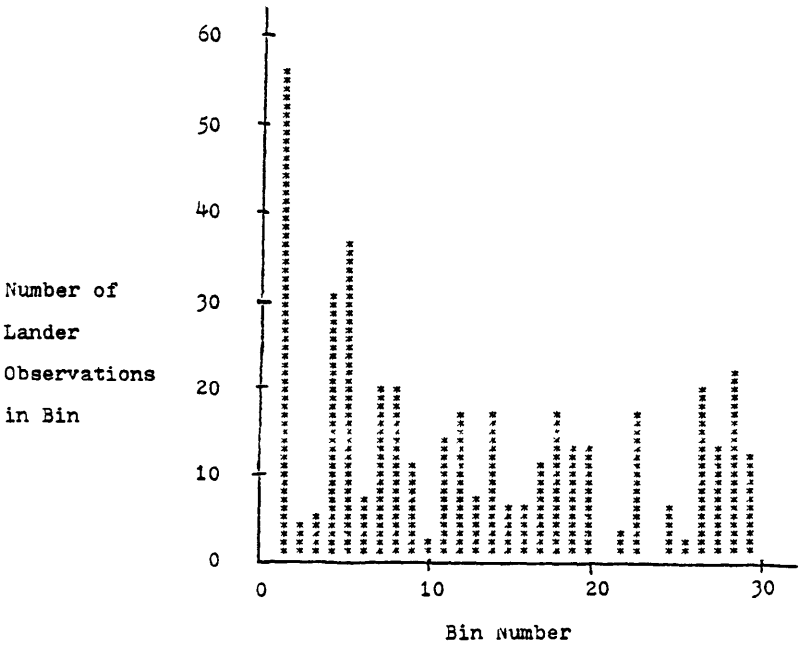

Figure 21a) HOG Output

Residual Scatter vs. Smoother Interpolation Time
Interpolation time = |Thin Screen time - time of nearest SX observation|
410 Lander Range Residuals
Bin Width = 0.01 day (14.4 minutes)
Run AP-48F

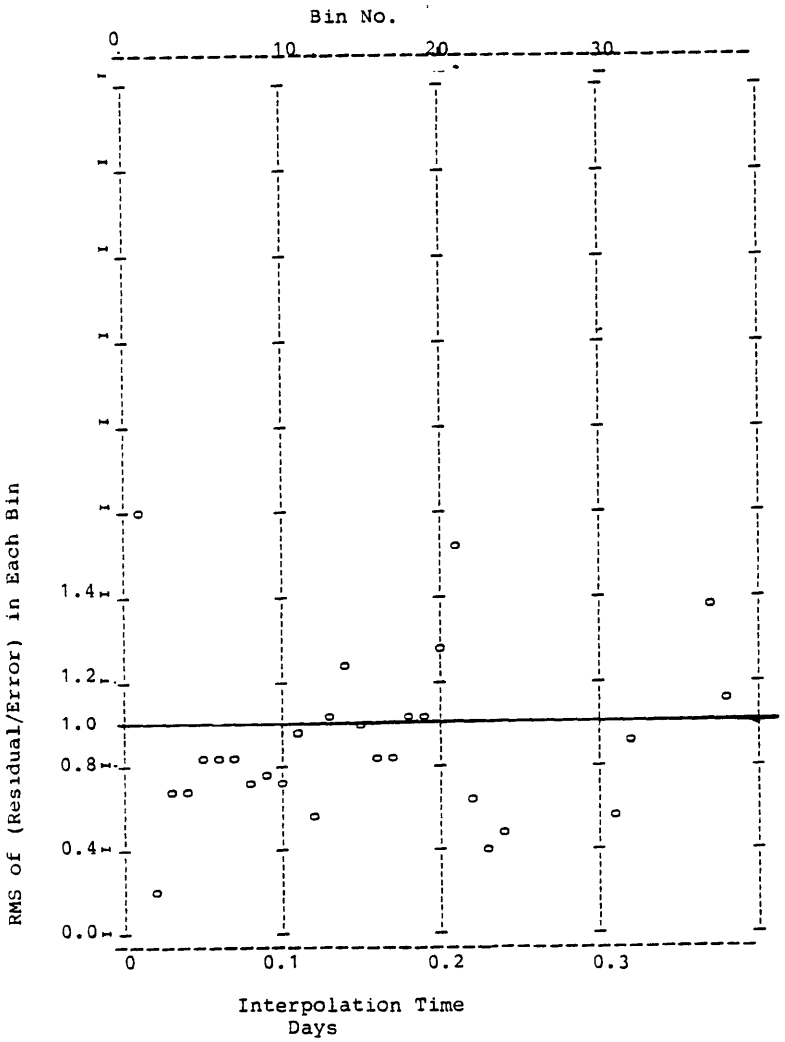

Figure 21 b) Histogram of number of Lander Obervations versus Smoother Interpolation Time for Run AP-48F.
Bin Width = 0.01 Day

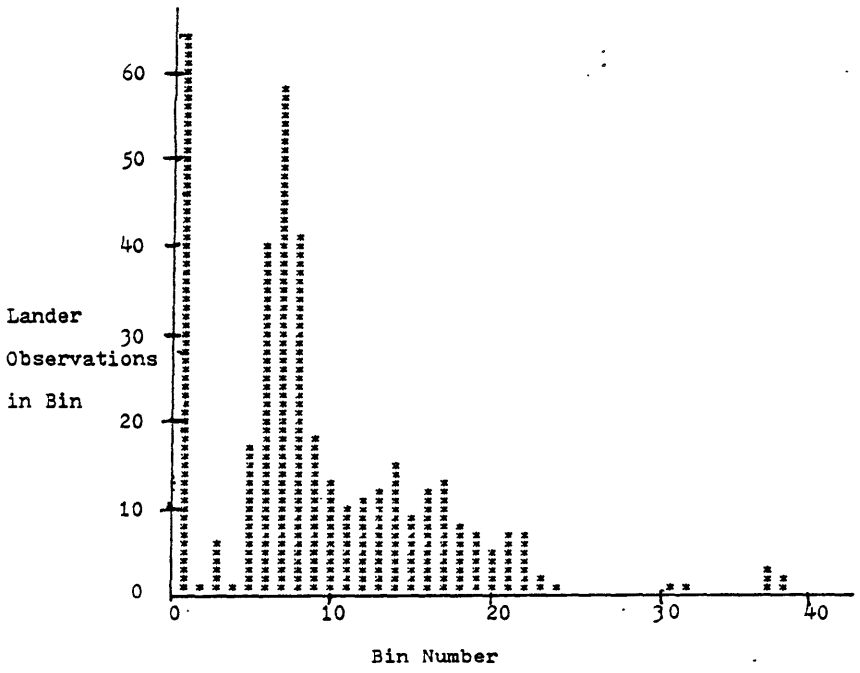

Figure 23a) HOG Output

Residual Scatter vs. Number of SX Range Observations Used in Interpolations
410 Range Residuals
Bin Width = 2 SX points

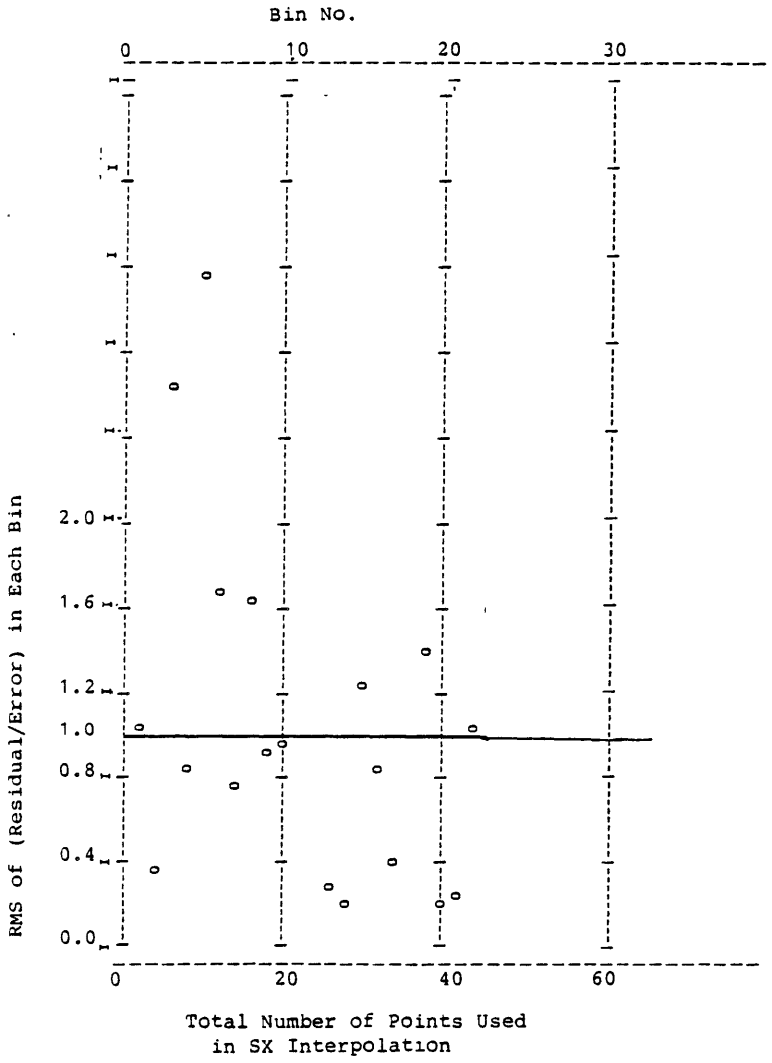

Figure 22 b) Histogram of number of Lander Observations versus number of SX delay observations used in interpolation for Run AP-48F.
Bin Width = 2 SX delay observations